Experimental Stark widths and shifts for non-hydrogenic spectral lines of ionized atoms

Cite as: Journal of Physical and Chemical Reference Data **5**, 259 (1976); https://doi.org/10.1063/1.555533
Published Online: 15 October 2009

N. Konjevic, and W. L. Wiese

Experimental Stark Widths and Shifts for Non-Hydrogenic Spectral Lines of Ionized Atoms

(A Critical Review and Tabulation of Selected Data)

N. Konjevic*

Institute of Physics, 11001 Beograd, P.O. Box 57, Yugoslavia

and

W. L. Wiese

Institute for Basic Standards, National Bureau of Standards, Washington, D.C. 20234

A critical review of all available data on the Stark widths and shifts for lines of non-hydrogenic ionized spectra has been carried out. The relevant literature compiled by the NBS Data Center on Atomic Line Shapes and Shifts was critically evaluated, and from this evaluation 54 papers were found to satisfy all requirements and thus selected for this review. The most important factors determining the quality of plasma sources, diagnostic techniques, and line profile and shift determinations are discussed in detail in the first part of this review. In the second part the data tables containing the selected experimental Stark broadening parameters are presented. The data are arranged according to spectra and elements, and these are presented in alphabetical order. The accuracy of the experimental data is estimated on the basis of guidelines developed during the review, and comparisons with theoretical results are made whenever possible.

Key words: Critically evaluated data; experimental; ionized spectra; Stark broadening parameters; Stark shifts; Stark widths.

Contents

*Part of this work was performed while the author was at the National Bureau of Standards.

1. Introduction

This review is to our knowledge the first attempt to critically evaluate and assemble the experimental material on Stark broadening parameters for isolated lines of ionized spectra. The experimental data have been largely acquired within the last 10 years and thus represent material obtained by comparatively modern techniques of plasma spectroscopy. The primary stimulus for this work has been the need for accurate and convenient determinations of electron densities in laboratory and stellar plasmas for which Stark broadening—provided reliable width parameters exist—constitutes a very attractive and convenient technique.

Practically all experiments reviewed here were designed to be checks on theoretical Stark broadening parameters; i.e., they were planned to specifically investigate the accuracy of the calculated parameters and to verify their theoretically estimated uncertainties. Therefore, we have taken into account the obvious importance of the theoretically calculated parameters and have always made comparisons with these parameters in addition to straight presentations of the experimental data. The theoretical parameters are all taken from the only general tabulation available – the one by Griem [1][1], which is based on earlier semiclassical calculations of the electron-impact broadening of ion lines by Jones, Benett, and Griem [2]. (These calculations do not include the usually insignificant ion (quasistatic) broadening.) The comparison with the theoretical data is also essential for comparing the results of various experiments done under different conditions since only the calculated line broadening parameters, in conjunction with relations giving the temperature as well as density dependence [1], can connect the different measurements.

In obtaining the literature sources for the experimental papers, we have put emphasis on completeness. We have used the references listed in the "Bibliography on Atomic Line Shapes and Shifts," NBS Special Publication 366 and its addenda [3], and have also made use of all later information available in the NBS Data Center on Atomic Line Shapes and Shifts. We have thus obtained all material through the end of 1974, at which point the tables were finalized. Papers available to us in preprint form by that time were included, too, and their exact references added later.

For the evaluation of the results and estimates of the uncertainties in each experiment, we have examined a number of critical factors which in our opinion most strongly influence the quality of the measurements. Principally, these factors arise in three areas of the experiment: (1) the plasma source and its properties, (2) the diagnostic technique, particularly the determination of the electron density, and (3) the line shape measurement technique including the unfolding of narrow profiles. Because of their crucial importance for the evaluation of the data, these factors shall be discussed below at some length.

During the initial evaluations, we noticed that a number of papers are clearly superseded by later work of the same group or that other papers are so incomplete in the reporting that no estimate of uncertainties could be made. Such papers were excluded from further evaluation. In other cases where the reporting (or the experimental work) has not been seriously incomplete, we have considered these papers but with a relatively low accuracy rating. For example, we have done this when it must be suspected that self-absorption or the apparatus width will be significant factors but when no check on these points has been reported.

It will be seen from the comparison tables and graphs that the accuracy estimates given in the literature are quite often too optimistic. Frequently, no overlap exists between the results of different authors within their stated uncertainty estimates, so that one has to conclude that at least one of the data contains further unaccounted-for uncertainties. Thus, we feel justified in being generally more conservative in arriving at our error estimates.

We hope that this critical review and the tabulation of experimental data will (a) provide a good summary of the present status of our knowledge, (b) induce improvements in the experimental work and its reporting, and (c) focus on the many additional needs in this field.

It is the intention of the staff at the NBS Data Center on Atomic Line Shapes and Shifts to commission future critical reviews on this subject when major additions and improvements in the data warrant it.

2. Critical Factors in the Stark Broadening Investigations

2.1. Plasma Sources

The ideal plasma source for Stark Broadening studies of ionic lines should be: (1) stationary, (2) homogeneous, (3) capable of achieving a relatively high excitation temperature ($\geq 10{,}000$ K) in order to obtain sufficient numbers of ionized atoms, and (4) capable of achieving a relatively high electron density ($1 \times 10^{16} - 1 \times 10^{18}$ cm^{-3}) in order to produce Stark broadening as the predominant and readily measurable cause of line broadening.

[1] Figures in brackets indicate the literature references.

Since such an ideal source is not available, a variety of plasma sources which partially satisfy these conditions have been used. In table 1 a list of the various utilized plasma sources is presented as well as the number of selected papers in which these have been used. In order to illustrate the usefulness of the different sources for investigations on various elements, the number of elements investigated with a particular plasma source is also given.

It is evident from table 1 that pulsed sources were mainly used. They usually satisfy the above conditions (3) and (4) and approximately satisfy condition (2). The most popular pulsed source was the electromagnetically driven T-tube.

In table 2 the ranges of electron densities and temperatures are listed which have been employed in the different plasma sources for the investigations of the Stark broadening of ionized lines.

TABLE 1. List of applied plasma sources

Type of plasma source	Electromagnetically driven T-tube	Low pressure pulsed arc	Plasma jet	Various types of arcs	Z-pinch	Gas driven shock tube	Other plasma sources
Number of papers	16	7	7	7	3	4	7
Number of investigated elements	11	8	4	5	6	7	7

TABLE 2. Electron density and temperature ranges for applied sources

Type of plasma source	Electron density range (cm^{-3})	Temperature range (K)
Electromagnetic T-tube	$(0.5–8.0) \times 10^{17}$	9,000–25,000
Low-pressure pulsed arc	$(0.3–2.0) \times 10^{17}$	14,000–40,000
Plasma jet	$(0.7–1.0) \times 10^{17}$	12,000–14,000
Various types of steady-state arcs	$(0.7–2.0) \times 10^{17}$	11,000–20,000
Gas driven shock tube	$(0.5–1.0) \times 10^{17}$	10,000–12,000
Z-pinch	$(0.3–4.0) \times 10^{17}$	25,000–35,000
Θ-pinch	4×10^{17}	60,000

a. Pulsed Plasma Sources—Shock Tubes

Electromagnetic T-tube. This plasma source was described previously in a number of articles [4]. It consists of a T-shaped tube (usually glass) with two electrodes protruding into the two opposite ends of the short arm of the "T." A condenser bank is discharged, via a spark gap, through the gas between electrodes. The return current path is put close to the discharge, and the electromagnetic interaction between them, as well as the pressure gradients, drive the ionized gas away from the return lead with such force that an intense shock wave is produced. Most of the plasma measurements have been carried out after the reflection of the shock from the reflector placed in the expansion tube. The spectroscopic observations are usually made 1–12 mm from the reflector.

Typical dimensions of the T-tubes are: expansion tube i.d., 16–38 mm; distance between electrodes and the reflector, 10–15 cm; and gas pressure, 1 torr.

The majority of the electromagnetic T-tubes for line broadening studies were of a design similar to that used first by Kolb [5]. Recently, Ervens and Berg [6] proposed a modification of the expansion tube with a "cookie-cutter" arrangement. In this way the replacement of the expansion tube, which becomes clouded after a number of shots, is simplified.

The discharge in an electromagnetic T-tube is usually driven by a low inductance capacitor bank with a capacity of the order of 1 μF charged up to 40 kV. The plasma duration after the reflection of the shock wave is typically a few tenths of a microsecond. Recently, larger and slower capacitors (7.5 μF [7] and 14 μF with an external inductance of 4 μH [8]) were used to obtain a more homogeneous plasma with a duration of a few microseconds.

Shot-to-shot reproducibility of the radiative intensity in most shock tube experiments has been found to be ± 15 percent or better and partially depends upon the type of working gas. Molecular gases (e.g., nitrogen, oxygen, and dichlorodifluoromethane) are much less reproducible than atomic ones (helium, neon, and argon). To improve the shot-to-shot reproducibility, RF preionization was used [6]. For example, Konjevic et al. [10] improved scanning reproducibility in dichlorodifluoromethane by 30 percent by using a 50 watt RF source for preionization.

Other shock-tube tubes. The gas-driven shock tube was employed in two Stark broadening studies of ionized sulfur and chlorine lines [11, 12]. Cold hydrogen was used to drive the conventional 7.5×10 cm ^{2} shock tube. The steady-state region in the stationary plasmas behind the first reflected shock varied in duration between 50–200 μs. By suitable selection of initial gas pressure and composition, it was possible to vary the plasma electron density between 2 and 14×10^{16} cm^{-3} while

keeping the temperature to the range 10.000–12.500 K.

In another experiment the parallel-rail shock tube was used as a plasma source [13]. Unfortunately, the details of this shock tube are given only in an unpublished Ph. D. thesis.

b. Pulsed Sources—Pulsed Arcs and Others

Low-pressure pulsed arcs. Since basically only three different pulsed arc sources [14–16] were used for investigations of Stark parameters of singly ionized lines, some details will be given on each source in table 3. The pulsed arcs all have in common that the plasma is generated by discharging a capacitor bank through a glass tube filled with gas at reduced pressure. In general, the shot-to-shot time reproducibility of the light intensity from low-pressure pulsed arc discharges is better than from electromagnetic T-tubes and is usually within ±5 percent.

Most investigations of the spatial homogeneity of the plasma were carried out by high speed photography. For example, in ref. [16] this check was done by taking photographs of the continuum radiation from the discharge (side-on) at various times by means of a Kerr cell shutter (with an exposure time of 30 ns) and a camera. Densitometric analysis of the photographs showed that the plasma was highly homogeneous in the axial direction (within ±4 percent). Also, the plasma length could be determined in this way with an accuracy of ±2 percent which was of importance for axial interferometric electron density measurements. A similar analysis was performed radially, and it was found that the plasma was approximately homogeneous for the chosen experimental conditions. This was also confirmed by scanning the profiles of some lines at different radial positions of the discharge, and no difference was observed in the shape and width of the observed lines.

TABLE 3. Characteristics of applied pulsed plasma sources

Ref.	Discharge vessel		Electrode material	Typical filling pressure (mmHg)	Capacitor bank (μF)	Typical operating		Typical duration of current pulse (μs)	Plasma parameters [a]	
	Internal diameter (mm)	Length (cm)				Voltage (kV)	Current (kA)		Electron density (cm^{-3})	Electron temperature (K)
14	40	10	C	10	200	4–10	36	60	$(1.0–7.0)\times10^{17}$	10 000–12 000
15	12 [b]	30	Al	10	16×5 [c]	12	14	90	2×10^{17}	30 000
16	24	20	Al, C	0.1	150	1–2	5–14	40	$(0.3–1.2)\times10^{17}$	20 000–40 000

[a] Values given in the two columns are typical and are not necessarily correlated.
[b] Diameter of the constricted part of discharge vessel was enlarged around the electrodes in order to reduce impurities.
[c] Lumped-parameter delay line.

(Observations of this type are strongly suggested for each experiment.)

Z-pinch. Basically, this is a low-pressure pulsed arc but with higher electric current so that the self-produced magnetic field causes pinching of the plasma column. In this way higher electron concentrations than in pulsed arcs can be achieved, which is of advantage when investigating the often narrow lines of multiply ionized atoms.

Pulsed capillary discharge. In two papers (originating from the same laboratory) a pulsed capillary discharge was used as a plasma source [17, 18]. The electrodes of the discharge were made of carbon, and they were pressed against a circular disk of a plexiglass containing at its axis an insert of calcium chloride [17] or aluminum hydride [18]. The diameters of the capillary were 3 and 2 mm, respectively.

The discharge was driven by a lumped-parameter delay line consisting of six capacitors of 80 μF each and coils of 3.6 μH inductance, giving a maximum discharge current of 10.2 kA. The current pulses were rectangular with 205 μs duration. Spectroscopic observations were performed side-on on the plasma flame protruding from the capillary. The flame was of good radial symmetry permitting the Abel inversion of the spectra.

Other pulsed sources. Two other pulsed plasma sources need to be mentioned for this review: (a) a pulsed discharge sliding along the surface of a liquid jet [19] and (b) the theta pinch [20].

(a) A condenser battery of 21 μF (inductance: 17.4 μH) charged up to 25 kV was discharged along the surface of a liquid jet of low conductance. The discharge current was not critically damped, the oscillations had a half period of 116 μs. The plasma, which surrounded a liquid column, was radially symmetric. Barium, investigated in this experiment, was introduced into the plasma by evaporation of the jet solution.

(b) The theta pinch is a well-known plasma source frequently used for investigations of plasmas. It was used [20] in an experiment set up to determine Stark broadening parameters of multiply ionized carbon lines. The small theta pinch arrangement included preioniza-

tion, a preheater, and a main discharge using a 25 kV, 3 μF condenser bank. The compression coil had a length of 30 cm and a diameter of 4 cm. The filling pressure was about 0.4 torr. Spectroscopic observations were made axially end-on. The magnetically compressed plasma typically had an electron density of 4×10^{17} cm^{-3}, a temperature of 60,000 K, and a lifetime of about 0.1 μs.

c. Stabilized Arcs and Plasma Jets

The two types of stationary plasma sources that have been used for Stark broadening studies are stabilized arcs and plasma jets. The plasmas are typically long, rotationally symmetric columns of cylindrical shape (arcs) or conical shape (plasma jets). Typical dimensions are 5 mm for the column diameter of wall-stabilized arcs and 100 mm for their length; the plasma jets are also about 5 mm in diameter and are 20–30 mm long. The high pressure (up to 150 atmospheres) gas-stabilized arc [21, 22] has much smaller dimensions, about 5 mm in length and 1–2 mm in diameter, because of its larger power requirements. A variety of different arc sources and plasma jets have been described in the literature, to which we refer for further details [23, 24].

The most attractive feature of arcs and plasma jets is their stationary behavior which permits long observation times and the application of slow photoelectric scanning techniques. The observed line profiles are therefore often precisely defined (see e.g., the line profiles illustrated later in this review). The extended operating times also permit accurate applications of various plasma diagnostic techniques. However, the range of plasma parameters and of diagnostic methods is more limited than for other sources (see also table 2). For example, for the wall-stabilized arcs the limited access to the arc channel and its small radial extension make applications of laser scattering techniques impractical.

To obtain accurate data with stabilized arcs and plasma jets, the following factors are most critical and have to be carefully investigated. Boundary layers in end-on measurements have to be taken into account by model estimates, or they need to be minimized by introducing the species under study into the middle part of the arc only, away from the cooler electrode regions [23]. If gas mixtures are used, careful attention must be given to maintaining a constant mixture ratio. Finally, side-on observations require application of an advanced Abel inversion scheme [23] in order to produce precise results. While the inversion constitutes a bit of data analysis work, it has the advantage that profile data are obtained over the whole radial range of electron densities, so that the dependence of line widths and shifts on the electron density is readily obtained.

2.2. Plasma Diagnostic Methods

The most critical part of the plasma analysis is the accurate determination of the electron density since the line broadening parameters depend linearly on it, except for small higher order effects such as ion broadening. The other quantity which also directly affects line broadening parameters is the plasma temperature, but the correlation with this quantity is a much weaker one.

In the following we shall discuss the critical factors involved in the principal methods used for the electron density and temperature determinations. The various spectroscopic approaches are well established, and we presume that the reader is familiar with them so that explanations will be kept to a minimum. For detailed discussions of these diagnostic techniques, we refer to a number of recent books and review articles [23, 25, 26]. However, the one essentially non-spectroscopic method often applied here, laser interferometry, is a rather recently developed technique which has not been reviewed in detail yet for the special conditions under which it is used in Stark broadening experiments. We shall, therefore, present an extended explanation of this important new technique in section 2.2.b.

a. Electron Density Determinations from Measurements of Stark Profiles

In approximately one-half of the papers, the electron density has been determined by measuring the Stark widths of spectral lines for which the broadening parameters are well established by theoretical calculations and measurements. These lines usually belong to species added in traces to the plasma rather than the main constituent. This diagnostic technique is a very attractive one since the measurements involved and the interpretation are quite simple (except, perhaps, for the somewhat laborious shot-to-shot scanning with pulsed sources), and the Stark widths are directly proportional to the electron density. (These advantages have, of course, also provided a major stimulant for preparing this review, insofar as it will contribute to identify additional reliable Stark width data for determinations of plasma electron densities.)

The most important points one has to consider in this diagnostic technique are corrections for possible effects of other broadening mechanisms, including instrumental broadening, corrections for possible self-absorption, and corrections for the continuous background under the line. Also, one has to assure that the line is truly isolated and not blended with any other weak line of the same species or impurities. The most desirable approach to determine a Stark width is to compare the whole measured profile with the theoretical one and find the electron density from the condition of best fit rather than from the simpler measurement of the halfwidth. This comparison has actually been performed sometimes in the experiments reviewed here (see, e.g., Chapelle et al. [27], Popenoe and Shumaker [28], and Yamamoto [29]).

The most accurate results are obtained from comparisons with the Balmer line H_β which is quite frequently used. Many experimental and theoretical studies

have established that precise halfwidth measurements on this line will yield electron densities to within 10 percent [1, 30]. For the He 3889 Å line, which has been applied only slightly less often, good agreement between measurements and theory has been found [1, 31], too, so that its line width parameter should be nearly as reliable as for H_β. However, the 5 percent accuracy estimate stated in ref. [32] appears to be overly optimistic.

Applications using other lines whose Stark width parameters have only been established by a single theoretical or experimental investigation are less reliable. This especially applies to the experimental data on a C I resonance line by Kusch [33], which is used in later work of Kusch and Pritschow [17] on Ca II and Heuschkel and Kusch [18] on Al II. As seen in another recent review [31], the measured Stark halfwidth for the C I line disagrees drastically with both theory and a more recent experiment, i.e., it is a factor of 6 larger than the theoretical value and a factor of 8 larger than another experimental result. As a consequence, the Ca II and Al II results by Kusch and coworkers are very suspect, and indeed, it is seen that their work again yields very broad line profiles, wider by about a factor of 5 than the other experimental results (see the Ca II and Al II tables). Hühn and Kusch [21] have recently remeasured some of the Ca II lines by applying different diagnostic techniques for the electron density determination, and the new line widths are appreciably narrower and come into fairly good agreement with other experimental and theoretical values.

b. Laser Interferometry

Since its development in 1963, laser interferometry has been continuously improved and may be applied now for measurements of electron densities in the range from 10^{10}–10^{18} cm^{-3} over optical path lengths of the order of 10 cm. Since laser interferometry was used in a number of the reviewed papers for the determination of electron density but has not been reviewed in detail yet for the high electron density conditions required for Stark broadening studies, it will be described here in some length.

It was found by King and Stewart [34] that if a mirror was placed on the axis of a laser beam, but outside the cavity, interference occurred between the reflected and incident light. If the external path length was altered by moving the mirror, then the whole laser output was amplitude-modulated at the Doppler frequency corresponding to the velocity of the mirror. The laser intensity undergoes one cycle of modulation for each complete wavelength change in the optical path. About 50 percent depth of modulation can be produced even with the mirrors several meters away when only a fraction of the output is reflected back into the cavity.

Hence, such a system is effectively an interferometer with the advantage that the laser is both the source of radiation and the detector of the interferometric fringes. It was first used by Ashby and Jephcott [35] to measure electron densities in plasmas, and the principle of operation can be best understood from figure 1.

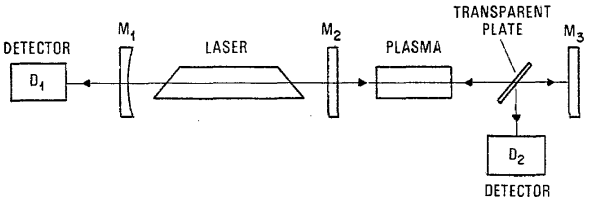

FIGURE 1. Schematic diagram of the laser interferometer (M_1, M_2, M_3 = mirrors).

The interferometer usually consists of a He-Ne laser with an external plane mirror M_3 which forms a Fabry-Perot etalon with laser mirror M_2. The external cavity contains the plasma whose index of refraction is to be measured. The interference fringes in the external cavity can be detected in two ways: (1) The intensity of the laser itself can be used to observe the fringes (with detector D_1). (2) Inserting a glass slide in the external cavity, a part of the interfering beam is reflected onto another detector D_2. In the first case the laser acts at the same time as source and detector, but in both cases the laser interferometer measures only a change in plasma refractive index and does not indicate the steady state conditions.

The advantage of the detection of fringes in the external cavity is a very high frequency response. In this way more than 50 resonances per microsecond have been detected [36]. Alternatively, if the laser is used as a detector, the signal is amplified which simplifies measurements, but the time response is worse. Which method is more advantageous depends, therefore, on the rate of change of the plasma refractive index.

The sensitivity of the basic laser arrangement depicted in figure 1 has been further improved by various methods: transverse modes are utilized [37, 38] which can be supported in the external cavity when M_3 is replaced by a spherical mirror; the third mirror M_3 is made to vibrate, producing fringes in the absence of the plasma, and when the plasma is pulsed, the fringes are shifted from their original positions [39, 40]; the plasma is placed in the laser cavity itself, and measurements of the plasma electron density are obtained in the range 10^{10}–10^{13} cm^{-3} by observing beat frequencies between two lasers where one is perturbed by the intracavity plasma [41–43]; a longer wavelength laser (CO_2 at 10.6 μm [44–46]) has been used in a laser interferometric arrangement.

Since in this review we are concerned with measurements of relatively high electron concentrations, typically in the range 10^{16}–10^{18} cm^{-3}, only laser interferometers with a plane external mirror, which are most suitable for this application, will be discussed further.

General reviews of the plasma refractive index and optical interferometry in plasma diagnostics have been given by Alpher and White [47], Martelluci [48], and Ascoli-Bartoli [49]. Therefore, only the pertinent details necessary for the understanding of laser interferometry will be presented here.

It is first important to realize that the laser only gives a variation in output when the plasma refractive index μ changes. Thus the electron concentration, even in a steady-state plasma, has to be determined during establishment or, alternatively, during interruption of the plasma state. Then the fringes arise due to changes in the concentration of all the component species; consequently, in a spectral region far from strong absorption lines,

$$\mu(t)-1=K_eN_e(t)+K_aN_a(t)+K_iN_i(t)+B(t). \quad (1)$$

Here the K values represent the refractivities and N's the densities of the electrons, atoms, and ions, respectively, and B is the contribution due to excited species. The latter term is not well known; however, following Alpher and White [50] one can take advantage of the large dispersion of the electron component and determine its concentration for a given plasma from the different number of fringes which are obtained at two different wavelengths. Thus,

$$\mu(\lambda_1)-\mu(\lambda_2)\cong\mu_e(\lambda_1)-\mu_e(\lambda_2)=$$
$$-4.49\times10^{-14}\,(\lambda_1^2-\lambda_2^2)\,N_e. \quad (2)$$

At this point it is convenient to introduce the number of fringes, f, produced by a plasma of length L placed in a Fabry-Perot cavity (fig. 1) for a change of refractive index $\Delta\mu$ at a wavelength λ:

$$f=\frac{\Delta\mu\cdot 2L}{\lambda}. \quad (3)$$

The factor 2 arises because the laser beam traverses the plasma twice. Hence, for the change of electron concentration ΔN_e (in cm^{-3}), eq. (2) gives. for two wavelengths,

$$\frac{1}{2L}(\lambda_1f_1-\lambda_2f_2)=4.49\times10^{-14}\,(\lambda_1^2-\lambda_2^2)\Delta N_e. \quad (4)$$

This relationship holds only for the simple laser arrangement; with an external concave mirror, the situation is more complex.

When the contribution of other plasma species to the refractive index can be neglected, it is possible to determine the electron density change in any time interval, in which the plasma refractive index varies, by using single wavelength interferometry:

$$\Delta\mu[\lambda]\cong\Delta\mu_e[\lambda]=4.49\times10^{-14}\lambda^2\Delta N_e, \quad (5)$$

i.e.,

$$\frac{1}{2L}\lambda f=4.49\times10^{-14}\lambda^2\Delta N_e \quad (6)$$

or

$$\Delta N_e=\frac{f}{4.49\times10^{-14}2L\lambda}. \quad (7)$$

Equation (7) is a good approximation for most of the low-pressure pulsed sources (arcs, Z- and Θ-pinches, electromagnetic T-tubes) where the electron concentration is in the range of 10^{16}–10^{18} cm^{-3}. Nevertheless, this should be evaluated, if possible, for each particular experimental condition. For example, in a low-pressure pulsed arc in argon with the plasma parameters:

plasma length	10 cm
maximum electron concentration	10^{17} cm^{-3}
and electron temperature	20,000 K,

the number of interferometric fringes due to the decay of electron density are 6.67 and 35.75 at 6328 Å and 3.39 μm. respectively. Although the sum of heavy particles in this plasma source (atoms, ions, including excited species) remains constant during the decay, it is much more difficult to evaluate its contribution to the variation of the refractive index. For an accurate calculation one must know the plasma composition as well as the mean electronic polarizability $\bar{\alpha}$ for each species. Both quantities are usually unknown, and therefore, we shall try only to estimate the contribution of nonelectronic species for our assumed experimental conditions. To evaluate the plasma refractive index, one can use the following relation [47]

$$[\mu-1]_i=2\pi\bar{\alpha}_in_i, \quad (8)$$

where n_i is the concentration of the particles per cm^3. Mean electronic polarizabilities for Ar I and Ar II are taken from [47]

$$\text{Ar I} \qquad \bar{\alpha}=1.98\times10^{-24}, \quad (9)$$

and

$$\text{Ar II} \qquad \bar{\alpha}=1.36\times10^{-24}. \quad (10)$$

If one assumes that at maximum electron density the plasma contains, aside from the electrons, only singly ionized atoms, then

$$\mu_{\text{Ar II}}-1=8.5\times10^{-7}. \quad (11)$$

At zero electron density, one has only neutrals whose refractive index is

$$\mu_{\text{Ar I}}-1=12.5\times10^{-7}. \quad (12)$$

Thus, the change of refractive index is

$$\Delta\mu = \mu_{Ar\,I} - \mu_{Ar\,II} = 4.0 \times 10^{-7}, \quad (13)$$

which corresponds to 0.13 and 0.024 of a fringe at 6328 Å and at 3.39 μm, respectively. Therefore, if one neglects the contribution of heavy particles to the plasma refractive index, an error of about ±2 percent at 6328 Å and ±0.06 percent at 3.39 μm results.

It is clear that at the time of maximum electron density in the plasma multiply ionized atoms and excited species also exist which have a larger mean electron polarizability [47]. However, their concentrations are much smaller than that of the singly ionized atoms in the ground state.

Although the above estimate shows that one-wavelength interferometry gives satisfactory accuracy for most of the plasma measurements, even at 6328 Å, it is always advisable to perform a two-wavelength measurement since the second measurement represents at the same time an additional accuracy and consistency check. For the atmospheric and higher pressure discharges (e.g., arcs and plasma jets), the contribution of heavy particles to the change of refractive index is not negligible and two-wavelength interferometry must always be performed. Furthermore, in some cases only axial measurements of electron density may be possible [51] due to large refractive index gradients and strong schlieren effects.

If eq. (7) is a good approximation, one can readily estimate from it the accuracy of the determination of electron densities by laser interferometry. The uncertainty in the plasma length introduces the largest error which is usually between ± 5 and ± 10 percent, if the plasma is homogeneous. The number of interference fringes (depending upon the plasma electron concentration and wavelength) is in the range 5–20 with a typical uncertainty of ± 0.2 of a fringe which corresponds to a relative error of ± 1–4 percent. Since these two principal errors are independent errors, the total error produced lies in the range from 5–11 percent, which is somewhat better than for many spectroscopic methods.

From the above arguments one may conclude that for low electron densities (smallest number of fringes and largest error in the determination of this number) it is advantageous to use a high sensitivity laser interferometer, e.g., with a concave external mirror or operating at long wavelengths, so that a large number of fringes would be produced. In all other cases the design of a plasma source which is highly homogeneous in the direction of observation and which has a well-defined plasma length contributes most significantly to obtaining high accuracy in laser interferometry. This argument implicitly stresses the importance of investigations of boundary layers along the interferometric beam.

Laser interferometry has become an attractive technique for measuring the electron density because it neither involves absolute intensity calibrations nor the sometimes laborious scanning of line profiles (e.g., of the Stark broadened H_β line). Furthermore, the alignment of the laser interferometer is very simple when working with a He-Ne laser operating at 6328 Å or at 6328 Å and 3.39 μm simultaneously. By counting the interference fringes, it is possible in a one-shot experiment (using single wavelength interferometry) to obtain the electron density in a pulsed plasma source along the laser beam path with an accuracy higher or equal to spectroscopic methods. Another major advantage is that the measurement does not depend on other properties of the plasma source, as is the case for some spectroscopic techniques which require the existence of local thermal equilibrium.

The main disadvantage of the laser interferometer is that it provides only an average electron concentration for that portion of the plasma volume which is traversed by the laser beam. Thus, to examine, for example, a radial distribution, the beam must be appropriately advanced across the test region, and this restricts rapid recording of the spatial distribution since the fringe patterns must be recorded at each point.

As far as classical interferometry (e.g., with a Mach-Zehnder instrument) is concerned, the sensitivity of the method is only one-half of the laser interferometric method employing a plane external mirror, due to the double path through the plasma. The applicability of classical interferometry is limited to transverse investigations of long plasmas, and the advantage of the long plasma length cannot be utilized due to schlieren effects which spoil the fringe pattern. Furthermore, one cannot take advantage of the increased sensitivity obtained with longer wavelengths due to the lack of suitable photographic technique for the far infrared. It may be possible to overcome this problem by using an infrared detector, but in this case the laser interferometric technique has the immediate advantages of (a) a simple optical alignment, (b) the possibility of using the laser as both a source and detector of radiation, (c) a double path system, and (d) the low cost of the laser compared with the classical interferometer.

c. Plasma Equations and Intensity Measurements

Several authors, principally Chapelle and coworkers [52, 53], have utilized this approach for argon, where because of the availability of many spectroscopic data it works particularly well. Local thermodynamic equilibrium (LTE) is assumed, and the plasma conservation and equilibrium equations [23, 25, 26]—such as the Saha equation, the condition of electrical charge neutrality, and the ideal gas law—produce in conjunction with line or continuum intensity measurements all the plasma composition data, i.e., the various particle densities and the temperature. While this method is a rather indirect approach to determine the electron density, it has nevertheless found frequent applications since it yields a complete plasma composition analysis and the

temperature simultaneously. It works especially well in high density stationary plasmas where, furthermore, checks with theoretical equilibrium criteria indicate that LTE is very closely approximated.

An important requirement for this method is that reliable atomic transition probabilities or continuum absorption coefficients must be available to properly utilize the line or continuum intensity measurements. In this respect, argon is a favorable case, because fairly accurate data for the above mentioned atomic quantities are known. Thus, for argon—as well as a number of other lighter elements—this approach is comparable in accuracy to the other methods discussed.

d. Miscellaneous Techniques

In some experiments [21, 22], the methods described under 2.2.a and 2.2.c have been combined to produce a redundancy of plasma data and thus judge their reliability from their mutual consistency. Such an approach is especially desirable if, in the individual diagnostic measurements, atomic data of uncertain accuracy are employed. In Murakawa's work [54] on Hg II, the Inglis-Teller method is used in which the electron density is estimated from the principal quantum number of the last observable line in a spectral series, an approach which is less accurate than the others.

e. Temperature Measurements

As stated before, the dependence of line broadening parameters on the temperature is not nearly as critical as on the electron density. Therefore, achieving a ±10 percent accuracy for this quantity appears to be fully adequate and is usually strived for. The methods principally involved are:

Relative line intensities within the same species. In this frequently applied method, the relative populations of several atomic states of different excitation energies are obtained from relative line intensity measurements. If the plasma is in partial LTE, the populations adhere to a Boltzmann distribution uniquely characterized by their excitation temperature, and this temperature T may thus be derived conveniently from a Boltzmann plot analysis [23, 25, 26]. Only the assumption of partial LTE among the excited atoms or ions and the knowledge of relative transition probabilities are required. Partial LTE normally exists for the high density plasmas applied here, and for many light elements, relative transition probabilities with accuracies close to 10 percent are available. The accuracy of this method depends critically on the number of lines available and especially on the energy spread between the excited atomic states involved, which should preferably be several times larger than kT. In favorable situations the temperature may be determined to 2–3 percent, while normally an uncertainty of about 5–10 percent must be expected.

Line-to-continuum intensity ratios. This technique may be regarded as a variation of the above discussed method insofar as the continuum replaces part of the lines. This method is more limited in its application because the required continuous absorption coefficients are generally not as available as atomic transition probabilities. Applications have been limited to cases involving helium as carrier gases [8, 55, 56]. This method is somewhat less accurate than that of the relative line intensities discussed before.

Intensity ratios of lines from successive stages of ionization of the same element. The intensity ratio of two lines from successive stages of ionization depends very sensitively on the temperature [23, 25, 26] since the temperature dependence of two such lines is very different due to a large difference in the excitation energies, of the order of 10–20 kT. (This difference includes the ionization energy of the lower ionization stage.) However, the electron density must also be determined, and the plasma must be in a state of complete LTE so that the two successive stages of ionization may be connected via the Saha equation. If this condition is met, as should be the case at high electron densities, then this method is a very accurate one for temperature determinations, superior to the first two methods discussed and comparable to the following method.

Plasma equations and intensity measurements. The method has already been discussed under electron density determinations (section 2.2.c). For all experiments in which the electron density is determined with this method, the temperature is simultaneously obtained from the analysis, too, which is an attractive feature of this technique.

2.3. Determination of Stark Profiles and Shifts

In principle, line shape measurements are straightforward. For the ideal case of a homogeneous steady state plasma, which is approximately realized in end-on observations on stabilized arcs and in very fast "snapshot" observations on homogeneous pulsed sources, one simply scans over the profile with a spectrometer of sufficient resolution. To carry out the very fast spectral scanning on pulsed plasmas, a rapidly oscillating Fabry-Perot spectrometer has been developed [57, 58]. Side-on observations of stabilized arcs and plasma jets are more tedious. In this case one has to obtain the intensity distribution over the cross section of the radially symmetric plasma for many fixed wavelength positions over the range of the line profile. Then, by applying an Abel inversion technique [23], one obtains the radial intensity distribution at each wavelength and can thus construct profiles for the radial positions of interest. An advantage of this method is that one may obtain profiles for a range of electron densities corresponding to the different radial positions; i.e., one may measure the functional dependence of line shape parameters on electron density from a single experimental run. (A graphical example is provided later.) In line shape deter-

minations from pulsed sources with standard monochromators, one must advance the instrument stepwise in small wavelength increments over the range of the line profile from shot-to-shot. Good reproducibility of the pulsed plasma source and a monitoring setup are required for this operation.

Line shifts are measured by comparing the investigated lines with unshifted reference lines generated in low-pressure lamps. This may be efficiently done by the photographic method because of the ease of recording spectra on photographic plates and measuring small wavelength differences. A special method applicable to pulsed sources is to use as the reference line the line emission from this same source at a very late stage of the discharge, when the electron density has decreased to a very small value [59–61]. (An example will again be illustrated later.)

The line shapes are usually the result of several broadening factors, from which the Stark profile component has to be isolated and retrieved. While the experiments have obviously been designed such as to have Stark broadening as the dominant cause of the width, conditions can rarely be made so ideal that all other broadening factors become insignificant. The best one can normally do is to reduce these as much as possible to make Stark broadening the largest single factor and then account for the other factors by suitable analysis and models. For the line shifts, the situation is less complex insofar as van der Waals shifts are the only competing factor. According to theoretical estimates [25, 26], they may sometimes be significant, especially if the Stark widths are small.

Unexpectedly, we found that the reporting on the measurement of line shapes and shifts and considerations of competing factors have often been done somewhat carelessly in the literature. About one-half of the 54 papers utilized for this critical compilation were incomplete in the reporting of possibly significant factors affecting the line shapes.

Most often, statements were missing about possible self-absorption effects and Doppler broadening. Since we could not determine if an experiment has been deficient on these points or if only the reporting was incomplete, we could not make a meaningful judgment on the data in this respect; to be on safe grounds, we made the assumption that these factors were not considered and, therefore, lowered our accuracy estimate by an amount which accounted for the estimated significance.

Before discussing the significant factors which may influence the observed line widths, it is useful to assemble some numbers for the various line width contributions encountered in some representative experiments. This is done in table 4, which shows that Stark broadening, while being a major contributor, is for all examples not the only important factor involved. Doppler as well as instrumental broadening are often comparable in magnitude, while the contributions from van der Waals and resonance broadening are normally estimated to be much smaller, and natural line broadening may always be neglected. With these numbers for orientation, we shall now examine the significant influences on the line shapes.

a. Instrumental Profiles

The standard practice to determine the apparatus profile of a spectrometer is to scan over a line whose intrinsic width is very small compared to the apparatus width so that the latter determines its shape. Typically, such narrow lines are obtained from low-pressure discharges, like Geissler tubes or hollow cathode lamps. The instrumental line shapes thus obtained are usually approximately Gaussian profiles. Since the Stark profiles are to a very good approximation of dispersion or Lorentzian shape, the well-known Voigt profile analysis [25, 26, 62] can be applied to derive the Stark width from the total observed width. A number of authors have also included in this analysis the Doppler width, which is readily derived from the temperature of the plasma [62]. Since Doppler broadening may be considered another independent cause of line broadening, which contributes—like instrumental broadening—a Gaussian profile, the two Gaussian profiles may be convolved. They again produce a Gaussian profile with a width equal to the root of the sum of the squares of the individual widths [25, 26, 62]. This resultant width may then be entered into the Voigt profile analysis to determine the Stark width as before.

For the plasma temperature range from about 10,000 K to 30,000 K and the elements and lines covered in these experiments, the Doppler halfwidths vary from about 0.2 Å for some lines of the lightest elements to about 0.02 Å for a Hg II line. The Doppler widths often constitute a significant contribution to the overall line width; nevertheless, in about 20 percent of the reviewed papers, Doppler broadening has not been reported so that we could not ascertain if it was considered. In these cases we have estimated the Doppler widths for the stated experimental conditions and have enlarged the error estimates accordingly.

In a few experiments [8, 13, 55, 63, 64], a fast oscillating Fabry-Perot interferometer has been employed for the line profile measurements. The determination of the apparatus function is in principle similar to the approach just described above, but the analysis and deconvolution procedure is more complex. A detailed description is given by Jones et al. [8].

Chapelle and coworkers have, in some of their recent work [27, 65], virtually eliminated the instrumental broadening contribution by using grating spectrometers in high orders (12^{th}–15^{th} order). They thus achieved a very high resolution, i.e., an instrumental width of about 0.03 Å, which is typically one-tenth or less of their observed Stark widths.

TABLE 4. (Full) Halfwidths due to various broadening mechanisms for some representative experiments

Author	Kusch [33]	Bridges & Wiese [82]	Chapelle et al. [52]	Yamamoto [29]	Jaeger [19]	Jones et al. [8]
Line	C II 2992 Å	S II 5027 Å	Ar II 4426 Å	Ca II 3934 Å	Ba II 4130 Å	Mg II 2802 Å
Temperature (K)	12800	11100	13000	11600	13200	18500
Electron Density (cm^{-3})	10^{17}	7×10^{16}	10^{17}	6.4×10^{16}	10^{17}	10^{17}
Halfwidths (in Å):						
Stark	4.00	0.39	0.40	0.079	1.24	0.044
Doppler	0.07	0.07	0.06	0.048	< 0.043	0.056
Apparatus	≈ 0.15	0.15	0.03	0.02	[a]	[a]
van der Waals (estimated)	< 0.025[b]		0.4×10^{-4}		< 0.015[c]	$\approx 4 \times 10^{-4}$
Resonance (estimated)	$< 0.8 \times 10^{-4}$					$< 4 \times 10^{-5}$
Natural[d]	$\approx 1 \times 10^{-4}$	$\approx 0.4 \times 10^{-4}$	$\approx 1 \times 10^{-4}$	$\approx 1.2 \times 10^{-4}$	$\approx 4 \times 10^{-4}$	$\approx 1.1 \times 10^{-4}$

[a] Not explicitly stated, but taken into account.
[b] According to figure 5 of Kusch's paper, the neutral hydrogen density is about 5 times higher than the electron density.
[c] Jaeger states that relatively high concentrations of neutral hydrogen and oxygen atoms are present ($N_H/N_{Ba} \approx 560$).
[d] Estimated from atomic transition probabilities tabulated in refs. [88, 89, 90].

b. van der Waals, Resonance, and Natural Line Broadening

The broadening produced by these mechanisms is usually not significant for the reviewed papers. Natural line broadening is always less than 10^{-3} Å and therefore completely negligible (see estimates in table 4). Furthermore, since the plasmas are ionized to an appreciable degree, the electron density is comparable to the neutral density, and electron impact broadening is dominant. Many authors have therefore not discussed the broadening by neutral particles. In a few experiments where a large number of neutrals are present (e.g., in the Ba II experiment of Jaeger [19], the density of (mostly) neutral hydrogen is 560 times that of (mostly) ionized barium), estimates for the line widths produced by van der Waals and resonance broadening have been made using rather approximate theoretical expressions [25, 66–68]. From these formulas one finds that for typical experimental conditions van der Waals widths are about a factor of 100 smaller than the Stark widths (see table 4). Similar, even more extreme ratios are obtained for resonance broadening which, furthermore, applies only to lines whose upper or lower state has an allowed transition to the ground state.

While these checks are sufficient for order of magnitude estimates, they will most certainly not suffice for cases where van der Waals broadening is estimated to become comparable to Stark broadening results, and experimental comparisons for such situations [21, 22] show that the early Lindholm-Foley [67, 68] theory often disagrees strongly with the measurements. For more recent and presumably more advanced theoretical data on van der Waals broadening, the line broadening bibliographies [3] issued by NBS should be consulted, which contain several new entries.

c. Self-Absorption

Self-absorption will have the effect of distorting and especially broadening a line and will, therefore, produce an apparent width which is too large. If the self-absorption originates mostly from cool boundary layers of much lower electron density and if the spectral resolution is sufficient, the line center exhibits readily recognizable self-reversal. But more often, self-absorption (especially when it originates within a homogeneous plasma layer) will only slightly distort the shape of a dispersion profile, even when it is very appreciable, as was borne out by a recent analysis [31]. Thus, it is normally very difficult to judge the amount of self-absorption from the observed shape of a line. In fact, good adherence of Stark broadened lines to dispersion shapes may have sometimes led authors to the false conclusion that line shapes have not suffered self-absorption.

A variety of well-established techniques exists to determine the presence of self-absorption effects. Particularly straightforward is the method of checking line intensity ratios within multiplets which are expected to adhere closely to *LS*-coupling. The well-known ratios for *LS*-coupling line strengths [67, 70] are taken as the basis to which the observed line intensity ratios are compared, and a reduction in the observed intensity of the strongest line in a multiplet relative to a weaker one indicates that self-absorption is present. For example, one must suspect that some self-absorption

is present in the Be II doublet presented by Sanchez et al. (fig. 2 of ref. [55]) since the intensity ratio of the lines is only about 1.8:1 instead of the 2:1 ratio expected from *LS*-coupling. (Since the lines in a multiplet have very nearly the same shape and width according to the theory, the ratio may be found by simply comparing the peak heights.)

A modification of this check is to vary the concentration of the species under study and look for variations in the intensity ratio (and in the line widths) with increasing concentration. Another popular technique to check for self-absorption is to double the optical path length by placing a concave mirror at its focal point behind the plasma and to find out if the increase in signal, except for reflection and transmission losses, also doubles. Preferably, one scans over the profile of the line and observes if the profile is proportional everywhere, by the same factor, to the profile obtained without the mirror in place. Self-absorption is present if the proportionality factor is not maintained for the high intensity region near the line center but instead becomes smaller. If the optical depth τ is not large ($\tau < 1$), one may correct the measured intensity to the limit of an optically thin layer [62].

Still another method consists of (a) calculating the intensity that would be emitted by a blackbody of the plasma temperature at the wavelength of the line peak and (b) comparing this with the actually observed (absolute) intensity at the line peak. If the observed peak intensity is not far below the calculated blackbody limit, this intensity ratio may, within a certain range (< 0.6), be used to apply corrections to the line profile.

In conclusion, we would like to emphasize that self-absorption can be a critical factor and should be given more attention in future experiments. We found unexpectedly that in about one-quarter of the reviewed papers no mention of self-absorption checks had been made. Since these checks are especially critical for resonance lines where self-absorption effects are most likely to occur, we had no choice but to lower accuracy ratings in all these cases. We feel, for example, that the very large Stark widths determined by Kusch and coworkers for Ca II [21] and Al II [17] lines may be to a good part explained by undetected self-absorption effects in another experiment by Kusch [14]. These effects have probably distorted [31] his experimental Stark width parameters for the C I 2478 Å resonance line used for the electron density determination in the above experiments.

d. Plasma Source Effects

Stark profiles may be distorted by the presence of cooler boundary layers or spatial and temporal inhomogeneities in the plasma over volumes and times for which no resolution is provided. Spatial and temporal inhomogeneities include those that may arise when materials are introduced into plasmas by evaporation from the electrodes or as dust from the walls. Any such unaccountable plasma source deficiencies will produce profiles which may be considered as superpositions of several components with different Stark widths. Some errors may be partly compensated if, for example, the Stark broadening of a reference line is used for the determination of the electron density, since it will suffer from the same defect. Often, this "superposition" of profiles is likely to give Stark widths which are smaller than the true width since regions of lower electron density will predominantly contribute to the center of the line and thus raise it. While the papers utilized for this critical compilation usually contain quantitative checks and corrections on temporal and spatial inhomogeneities, sometimes the reporting is very vague—we quote: "the nearly homogeneous central part of the plasma," "essentially homogeneous," "nearly rectangular light pulses"—so that it is impossible to make judgments on the magnitude of the uncertainties involved.

e. Miscellaneous Distorting Factors

The observed line shapes may also be distorted by some other factors, among which the possibility of blending with nearby impurity lines and wrong positioning of the continuous background are most prominent. If strong magnetic fields are present, Zeeman splitting must be taken into account. Finally, one must consider that the photographic technique is significantly more uncertain for the determination of line profiles than the photoelectric technique because of the complicated conversion process from film densities to radiation intensities, which involves a logarithmic dependence between these two quantities. In contrast, photoelectric signals are, over a wide range, directly proportional to radiative intensities.

3. Description of the Data Tables and General Discussion of the Results

3.1. Description of the Tables

Each data table is preceded by special remarks on the utilized papers. Then, in tabular form, the key factors for each selected experiment—i.e., the plasma source, the diagnostic technique, and the determination of the Stark profile—are described by a short phrase or remark for quick orientation, and the chosen references are listed. The remarks made on the determination of the actual Stark profiles and shifts are usually of critical rather than descriptive nature.

The data tables basically contain four pieces of information. In the first three columns, the investigated transitions are identified spectroscopically by their transition array, i.e., by quantum numbers and multiplet designations and, in addition, also by their wavelengths

(given in Angstrom units). The multiplet numbers refer to the running numbers in the multiplet tables by Moore [71], and the transitions are listed in order of increasing lower and upper quantum numbers.

The second part of the table, comprising columns 4 and 5, contains the temperature and electron density values at which the Stark widths and shifts have been determined. Frequently, the actual experimental conditions, especially the electron density, have not been stated by the authors, and, instead, the line shape data are presented at a reference electron density—usually 10^{17} cm^{-3}—to facilitate the comparison with the calculated widths and shifts. In most cases we had no choice but to list this reference density to which the experimental data had been reduced by using the theoretical scaling law.

In the third part of the table, the measured Stark halfwidths, w_m, and shifts, d_m, and the ratios of measured-to-theoretical widths, w_m/w_{th}, and shifts, d_m/d_{th}, are presented. The experimental Stark widths always represent full halfwidths and are arrived at *after* corrections for other broadening mechanisms, etc., have been made. The experimental Stark shifts, however, are usually identical with the observed shifts, i.e., the shift data contain no corrections since it is assumed that no other mechanism causing the line shifts besides Stark broadening is effective. The only two exceptions are the experiments by Helbig and Kusch [22] and Hühn and Kusch [21], performed with high pressure arcs, where the density of (foreign) neutral atoms is very high (up to 7×10^{19} cm^{-3}), 200 times larger than the electron density. Thus, van der Waals shifts are appreciable in this case and are separated from the Stark shifts by applying theoretical density and temperature relationships which are different for the two broadening causes.

The theoretical width values used in the experiment/theory ratios are from the tabulation by Griem and coworkers [1, 2], which is the only comprehensive set of calculated data available. The theoretical width data are for the electron impact width only, i.e., the usually very small additional width caused by ion broadening is neglected. The comparison with the theoretical data has been primarily done to make possible consistency checks between the experimental data for different elements and to obtain a general judgment on the reliability of the calculated parameters, since these should find many future applications.

In the final part of the table, our estimated uncertainties in the data are presented, and the references are identified. We have subdivided the uncertainties into four ranges and coded these by letters, and we have made further differentiations in the material by singling out slightly better pieces of data among several similar ones by assigning plus signs (+) to indicate our first choices. The letters represent the following:

A = Uncertainties within 15 percent,
B = Uncertainties within 30 percent,
C = Uncertainties within 50 percent, and
D = Uncertainties larger than 50 percent.

We summarize the reasons for the choice of our error limits in section 4.

3.2. Instructive Illustrations

A number of papers contain particularly instructive illustrations on profile and shift measurements, as well as very informative graphical data comparisons. As an example for precise profile measurements, we reproduce a graph from a paper of Chapelle et al. [27] in figure 2.

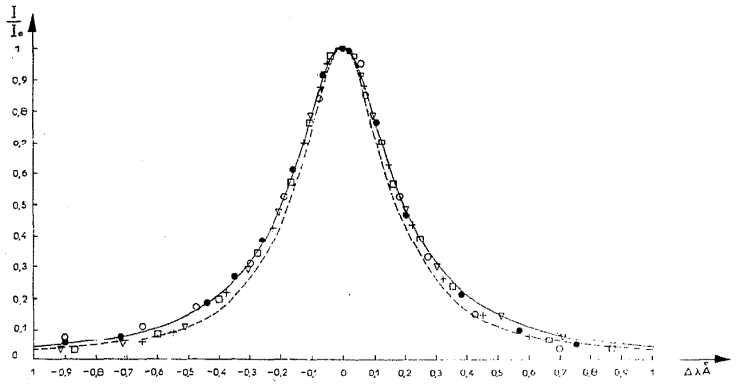

FIGURE 2. Stark profiles of five lines of the Ar II multiplet $4s\,^4P$–$4p\,^4D^\circ$ (+ 4330.18 Å, ▽ 4348.06 Å, □ 4331.20 Å, ○ 4379.67 Å, ● 4426.01 Å), from the measurements of Chapelle et al. [27]. The broken line is an (average) theoretical profile calculated according to a semiempirical theory by Griem [75].

These workers have used a grating spectrometer in the $12^{th} - 15^{th}$ order and thus obtain a very high spectral resolution (200,000) and a linear dispersion of about 0.4 Å/mm. Interference filters are utilized to prevent the overlapping of orders. The obtained line profiles are negligibly distorted by instrumental broadening (which is about 0.02 Å) but are, of course, still subject to other broadening mechanisms, principally Doppler broadening. For the case of the argon lines determined, Doppler broadening amounts, however, to only 10 percent of the Stark broadening, so that according to the Voigt profile analysis [62] the observed width is affected by no more than 1 percent. Thus, figure 2, which is a composite picture of five lines of the same Ar II multiplet, essentially represents a purely Stark broadened line profile.

Another instructive line profile (fig. 3) is reproduced from the paper by Jalufka and Craig [32]. The profile

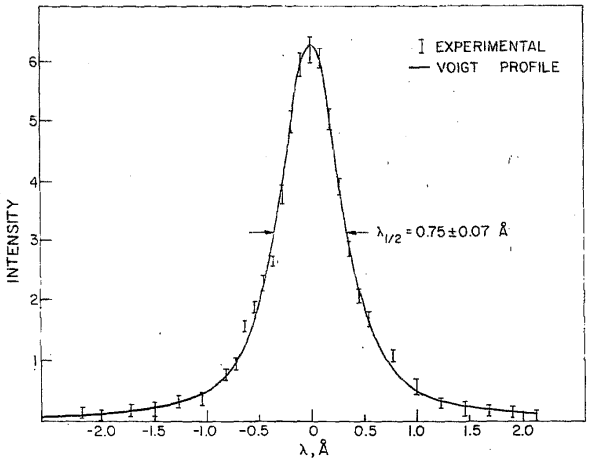

FIGURE 3. Experimental profile of the 3995 Å N II line, from the work by Jalufka and Craig [32]. A Voigt profile is fitted to the experimental data points.

for the 3995 Å line of N II is obtained from shot-to-shot scans with an electromagnetic T-tube. While the precision is not as high as in the preceding example, nevertheless a well-defined profile is obtained. The observed line shape contains appreciable instrumental broadening, which has been found to be of Gaussian shape. Since the Stark profile is Lorentzian, a Voigt profile is expected for the observed line shape, and, indeed, the fit to such a Voigt profile is seen to be very good. Part of the Gaussian component is probably also due to Doppler broadening, which the authors do not mention in their discussion.

Two illustrations of shift measurements are presented in figures 4 and 5. In figure 4, which is from a paper by Blandin et al. [65], the shift (to a shorter wavelength) of the Ar II 4806 Å line is shown. The trace for the plasma-broadened Ar II line emitted from a plasma jet is recorded with a high resolution spectrometer having

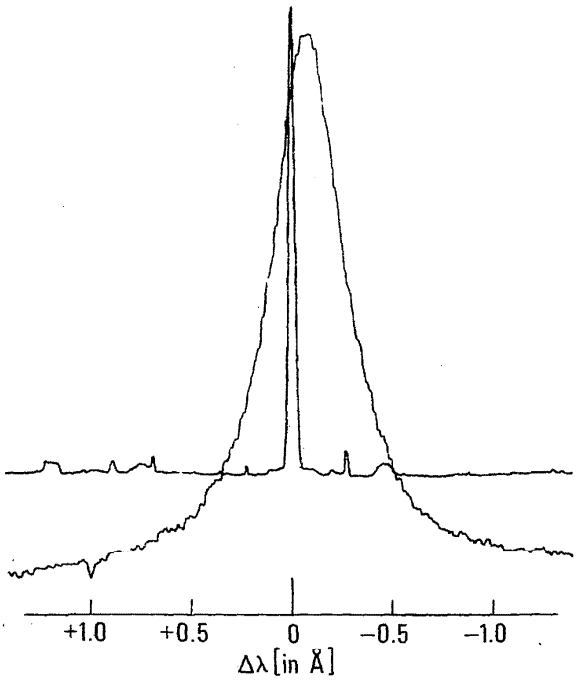

FIGURE 4. Violet shift of the Ar II 4806.07 Å line, from Blandin et al. [65]. The plasma broadened and shifted line is compared with the same, but narrow and unshifted, line of the Ar II spectrum as produced with a low-pressure hollow cathode discharge.

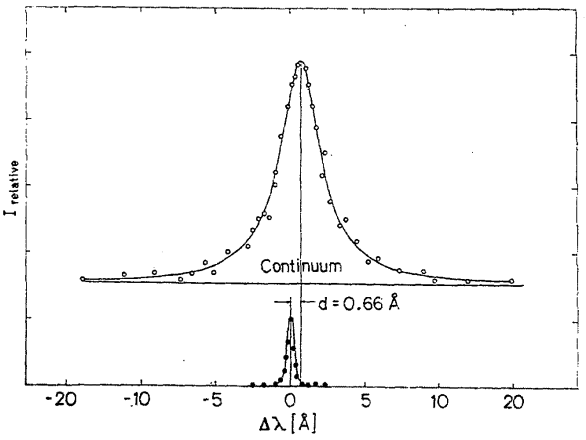

FIGURE 5. Two experimental profiles of the 4305.5 Å Sr II line obtained in a pulsed discharge at maximum electron density. 3.40×10^{17} cm $^{-3}$, (●), and 50 μs later (●) at an electron density smaller than 10^{15}cm $^{-3}$ from Puric and Konjevic [60].

a linear dispersion of 0.3 Å/mm and is the relatively broad shape with the lower background. The narrow reference line is the same argon line produced by a low-density hollow cathode lamp. The recording of the two lines is presumably done simultaneously (though not stated) by running both sources at the same time and

employing a half-silvered mirror to merge the two optical beams.

A different procedure for measuring line shifts has been developed by some other authors. Figure 5, taken from a paper by Puric and Konjevic [60], shows a shot-to-shot scan of the 4306 Å Sr II line analyzed for two different times during a pulsed discharge. The strong broad profile of the line is obtained at the time of the maximum electron density (about 3×10^{17} cm^{-3}), while the narrow weak profile is obtained 50 μs later, when the electron density is reduced to less than 10^{14} cm^{-3} and the Stark shift, compared to the first condition, is negligible. (The van der Waals' shift, too, is estimated to be very small, of the order of 10^{-3} Å or less, because of the low neutral densities ($\approx 10^{16}$ cm^{-3}).)

The next illustrations are taken from the stabilized arc measurements of Popenoe and Shumaker [28] and show the dependence of the halfwidth (fig. 6a) and shift (fig. 6b) on electron density for the 4806 Å Ar II line. The variation in electron density is obtained as a result of side-on measurements and the application of an Abel inversion procedure, which produce a range of densities corresponding to the different radial positions. The theoretically predicted linear dependence of the Stark width on electron density is seen to be well confirmed.

In the following six figures, 7–12, which may be considered updated and corrected versions of figures given by Roberts and Barnard [61] and Hadziomerspahic et al. [72], the experimental data on the (full) Stark halfwidths and shifts for resonance lines of the alkaline earths and their dependence on temperature are presented. Also included for comparison are theoretical data, i.e., the semiclassical calculations by Jones, Benett, and Griem [1, 2] (always for the electron impact widths) and the results of other special recent calculations [55, 73–78] for the alkaline earths. The figures

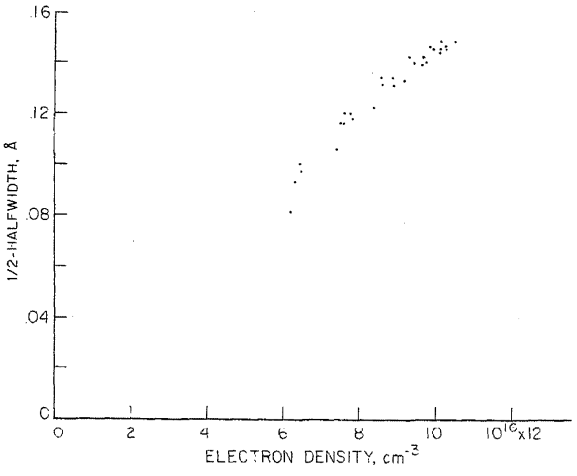

FIGURE 6a. Dependence of (half) halfwidth on electron density for the Ar II 4806 Å line, from the (side-on) arc measurements by Popenoe and Shumaker [28].

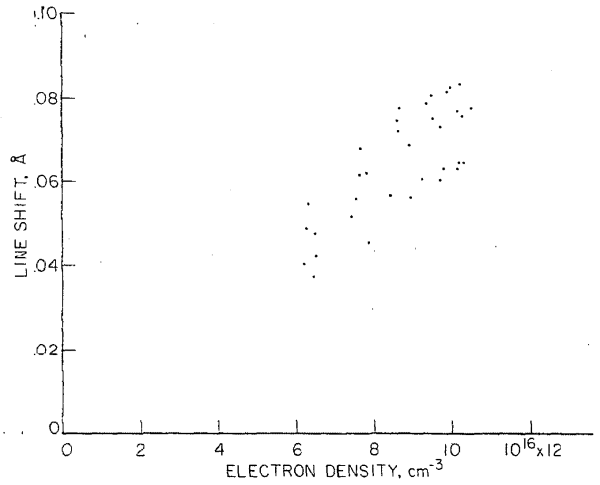

FIGURE 6b. Dependence of the blue shift of the Ar II 4806 Å line on electron density, from the (side-on) arc measurements by Popenoe and Shumaker [28].

show some appreciable differences between the experiments and calculations [1, 2, 73–78], but exhibit also some disagreements between the experiments themselves outside their mutual error estimates.

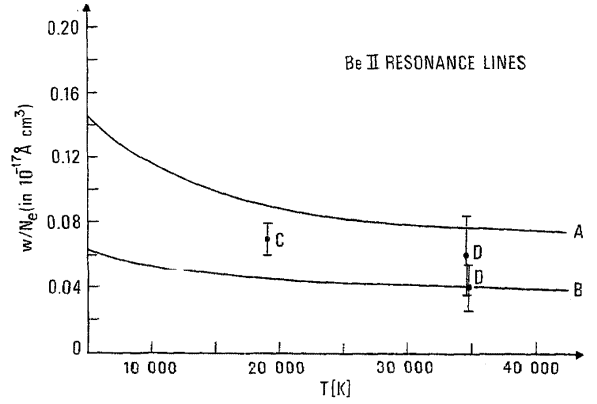

FIGURE 7. Measured and calculated (full) Stark halfwidths for the resonance lines of Be II (3130.4 Å and 3131.1 Å), normalized to $N_e = 10^{17}$cm^{-3}, as a function of temperature.

Curves: A = semiclassical calculations by Jones et al., Griem [1, 2]; B = quantum mechanical calculations by Sanchez et al. [55]; Experimental points: C = Sanchez et al. [55]; D = Hadziomerspahic et al. [72]. The error flags represent the authors' uncertainty estimates.

In particular, figures 8 and 9 show that the experimental width results of several authors do not overlap within their estimated mutual error limits. We refer specifically to disagreements for Mg II between Chapelle and Sahal-Brechot [53] and Jones et al. [8], on one hand, and Roberts and Barnard [61] on the other hand; and for Ca II, between Yamamoto [29] and Roberts and Eckerle [79], on one hand, and Chapelle and Sahal-Brechot [53], Hildum and Cooper [13], Jones et al. [8], Hadziomerspahic et al. [72], and Roberts and Bar-

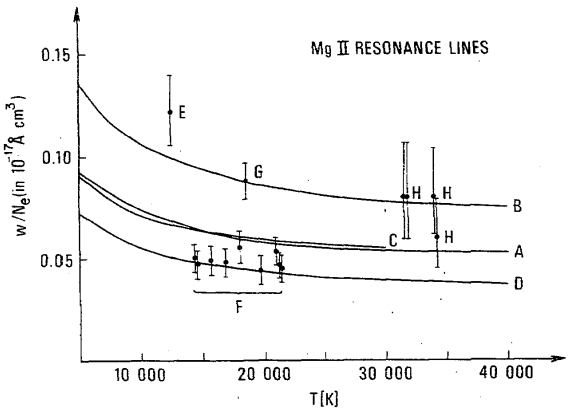

FIGURE 8. Measured and calculated (full) Stark halfwidths for the resonance lines of Mg II (2802.7 Å and 2795.5 Å), normalized to $N_e = 10^{17}\text{cm}^{-3}$, as a function of temperature.

Curves: A and B = semiclassical calculations by Chapelle and Sahal-Brechot [53] and Jones et al., Griem [1, 2], respectively; C and D = quantum mechanical calculations by Bely and Griem [76] (average for the two lines) and Barnes [77], respectively. Experimental points: E = Chapelle and Sahal-Brechot [53]; F = Roberts and Barnard [61]; G = Jones et al. [8]. H = Hadziomerspahic et al. [72]. The error flags represent the authors' uncertainty estimates.

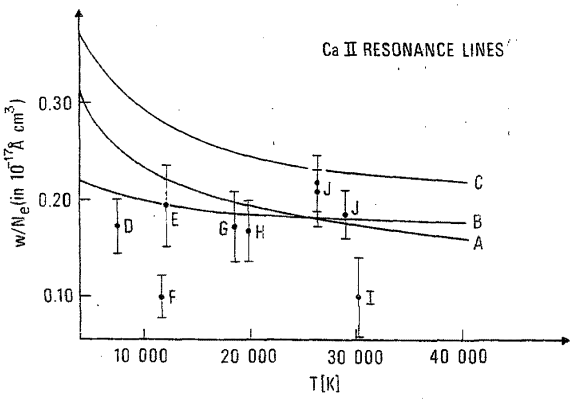

FIGURE 9. Measured and calculated (full) Stark halfwidths for the resonance lines of Ca II at 3933.7 Å and 3968.5 Å, normalized to $N_e = 10^{17}\text{cm}^{-3}$, as a function of temperature.

Curves: A = quantum mechanical calculations by Barnes and Peach [74]; B and C = semiclassical calculations by Sahal-Brechot [73] and Jones et al., Griem [1, 2], respectively. Experimental points: D = Baur and Cooper [87]; E = Chapelle and Sahal-Brechot [53]; F = Yamamoto [29]; G = Hildum and Cooper [15]; H = Jones et al. [8]; I = Roberts and Eckerle [79]; J = Hadziomerspahic et al. [72]. The error flags represent the authors' uncertainty estimates. The data of Kusch and Pritschow [17] lie outside the range of this graph ($w/N_e \approx 1.0$ at $T = 17{,}500$ K).

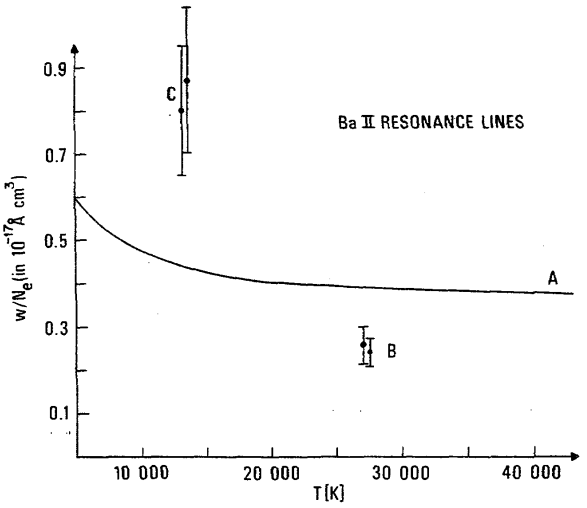

FIGURE 10. Measured and calculated (full) Stark halfwidths for the resonance lines of Ba II at 4554.0 Å and 4934.1 Å, normalized to $N_e = 10^{17}\text{cm}^{-3}$, as a function of temperature.

Curve: A = semiclassical calculations by Jones [78]. Experimental points: B = Hadziomerspahic et al. [72]; C = Jaeger [19]. The error flags represent the authors' estimates.

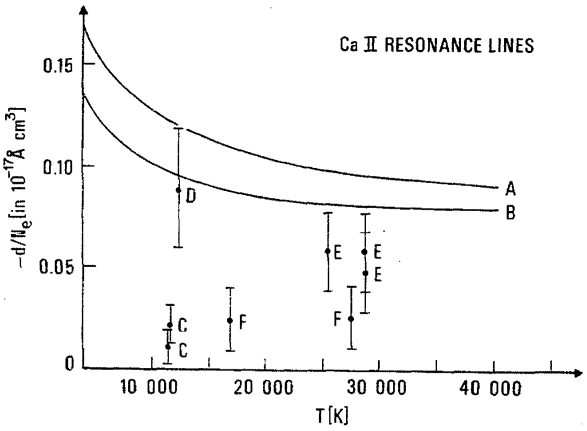

FIGURE 11. Measured and calculated Stark shifts for the resonance lines of Ca II at 3933.7 Å and 3968.5 Å, normalized to $N_e = 10^{17}\text{cm}^{-3}$, as a function of temperature.

Curves: A = semiclassical calculations by Jones et al., Griem [1, 2]; B = quantum mechanical calculations by Barnes [77]. Experimental points: C = Yamamoto [29]; D = Puric and Konjevic [60]; E = Hadziomerspahic et al. [72]; F = Roberts and Barnard [61]. The error flags represent the authors' uncertainty estimates.

nard [61] on the other hand. These examples apparently indicate that the authors' error estimates often have not included all the errors incurred, and that, therefore, error estimates should generally be more conservative.

The experimental data by Kusch and Pritschow [17] for the resonance lines of Ca II (outside the range of fig. 9) which are in strongest disagreement with all other results are also the ones which are most suspect. The plasma diagnostic technique of Kusch and Pritschow is based on the Stark width of a C I line measured earlier by Kusch [33], which itself is in strong disagreement with other measurements and theory [31] in the same direction as the disagreement obtained here. More recent measurements by Hübn and Kusch [21] on some other Ca II lines may be used to approximately correct the earlier results for the resonance line since both papers contain some lines in common. The Kusch and Pritschow Stark width for the Ca II resonance lines are then reduced by a factor of about 2.3 and thus come significantly closer to the other experimental data. Still, a difference of a factor of 2 remains, which may be due to self-absorption effects not considered for the —in

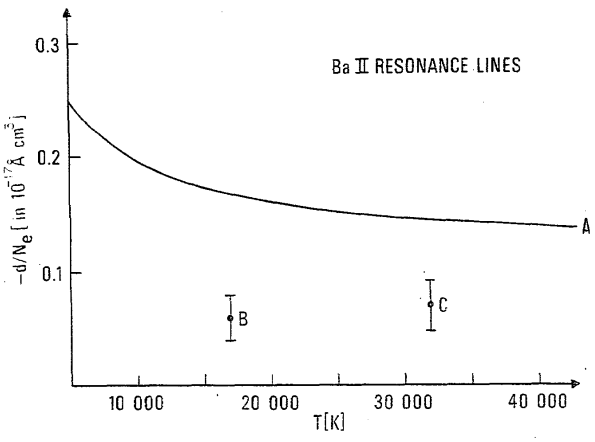

FIGURE 12. Measured and calculated Stark shifts for the resonance lines of Ba II at 4554.0 Å and 4934.1 Å, normalized to $N_e = 10^{17}$cm^{-3}, as a function of temperature.

Curve: A = semiclassical calculations by Jones [78]. Experimental points: B = Puric and Konjevic [60]; C = Hadziomerspahic et al. [72]. The error flags represent the authors' uncertainty estimates.

this respect—rather sensitive Ca II resonance lines.

3.3. General Discussion

Figure 2 contains important information on a question which has not been discussed yet, namely, how closely the Stark widths for different lines of the same multiplet agree. The figure shows that for five lines within a multiplet of Ar II the measured widths agree within the small experimental uncertainties, which are less than 5 percent. This result thus confirms a general prediction of the Stark broadening theory for isolated lines in cases where *LS*-coupling is a good approximation. Our tables contain a number of other cases where different lines within the same multiplet have been studied, for example: Be II lines [72]; C II [14]; O II [91]; O III [91]; Mg II [72]; Si II [80, 81]; S II [82]; Ar II [27, 52, 56, 63, 65]; Ca II [21, 72]; Ba II [19, 72]. In all these cases, the theory is confirmed, i.e., the lines in a multiplet have the same width within the experimental error limits. However, several exceptions exist, and it appears that width differences for lines of the same multiplet indicate deficiences in the experiments. The work in question is on Ca II [17], Cd II [83], Zn II [84], and S II and P II [11]. In some experiments we suspect the differences to be caused by self-absorption effects since the stronger line, which should be more self-absorbed, is broader than the weaker line in the multiplet.

The extensive shift measurements by Morris and Morris [85] on Ar II indicate that the multiplet rule is valid for the shifts, too. Within their estimated error limits, the same shifts are encountered within all multiplets.

4. Summary and Outlook

The principal elements in our critical evaluation of experimental Stark broadening data for isolated ionic lines have been the assessments of (a) the plasma sources (section 2.1), (b) the diagnostic methods (section 2.2), and (c) the measurement techniques for the line shapes and shifts (section 2.3). As discussed in detail in section 2, the discussions by the authors on points (a) and (b) were generally found to be sufficiently complete, and the estimated uncertainties appear to be realistic (but often on the optimistic side). However, significant deficiencies turned up in many authors' discussions on the Stark width and shift measurements (point (c)). To restate the most serious deficiency, approximately one-half of the selected papers did not contain any statements on the effects of either Doppler or apparatus broadening or possible self-absorption for conditions where the influence of these factors is estimated to be not negligible. Since we cannot be sure whether the missing statements are just an oversight in the reporting of the results or a true deficiency of the experiments, we have adjusted our accuracy ratings by an amount which we estimate will cover the additional uncertainty introduced.

Two additional factors guided us in our error estimates and caused us to be more conservative than many authors. These are, first, some discrepancies between experimental results outside the mutually estimated error limits, as is for example clearly seen in figures 8, 9, and 11, and secondly, the sometimes appreciable differences between the Stark widths of different lines within the same multiplet.

The experimental data on the Stark widths of isolated ion lines selected for this tabulation are found to be generally in agreement with each other within the error limits estimated by us. The best-rated data are recommended for plasma diagnostic applications.

A result of considerable practical value is the conclusion that the measured *widths* are generally in fairly good agreement with the comprehensive semiclassical theory developed by Griem and coworkers [1, 2], which confirms an earlier study by Jones on this subject [86].

This review also indicates the need for further experimental material, especially for high accuracy data, as well as for more completeness in the measurements and reporting. Most thoroughly investigated are the resonance lines of the alkaline earths and a number of prominent lines of Ar II, with fair agreement between the various experimental data as well as the experiments and calculations. Additional work most needed at this time is on the spectra of permanent gases, like O II or Ne II, for which many applications exist, as well as for higher stages of ionization.

5. References for Sections 1–4

[1] Griem, H. R., *Spectral Line Broadening by Plasmas*, Academic Press, New York (1974).

[2] Jones, W. W., Benett, S. M., and Griem, H. R., *Calculated Electron Impact Broadening Parameters for Isolated Spectral Lines from the Singly Charged Ions Lithium through Calcium.*

University of Maryland Technical Report No. 71-178, College Park, Maryland (1971).
[3] Fuhr, J. R., Wiese, W. L., and Roszman, L. J., *Bibliography on Atomic Line Shapes and Shifts (1889 through March 1972)*, Nat. Bur. Stand. (U.S.), Spec. Publ. 366; Fuhr, J. R., Roszman, L. J., and Wiese, W. L., *Bibliography on Atomic Line Shapes and Shifts (April 1972 through June 1973)*, Nat. Bur. Stand. (U.S.), Spec. Publ. 366, Suppl. 1, and Fuhr, J. R., Martin, G. A., and Specht, B. J., *Bibliography on Atomic Line Shapes and Shifts (July 1973 through May 1975)*, Nat. Bur. Stand. (U.S.), Spec. Publ. 366, Suppl. 2, Government Printing Office, Washington, D.C. (1972, 1974, and 1975)
[4] See, e.g., Kolb, A. C. and Griem, H. R., "High Temperature Shock Waves," in *Atomic and Molecular Processes*, D. R. Bates, Editor, Academic Press, New York (1962).
[5] Kolb, A. C., Phys. Rev. **107,** 345 (1957).
[6] Ervens, W., and Berg, H. F., Z. Phys. **222,** 180 (1969).
[7] Konjevic, N., Labat, J., Cirkovic, Lj., and Puric, J., Z. Phys. **235,** 35 (1970).
[8] Jones, W. W., Sanchez, A., Greig, J. R., and Griem, H. R., Phys. Rev. **A5,** 2318 (1972).
[9] Platisa, M., Puric, J., Konjevic, N., and Labat, J., Astroh. Astrophys. **15,** 325 (1971).
[10] Konjevic, N., Radivojevic, D., Cirkovic, Lj., and Labat, J., J. Phys. **B3,** 1742 (1970).
[11] Miller, M. H., *Thermally Insensitive Determinations of Transition Probabilities*, University of Maryland Technical Note BN-550, College Park, Maryland (1968).
[12] Bengtson, R. D., *The Measurement of Transition Probabilities and Stark Widths for C* I, *F* I, *Ne* I, *Cl* I, *Cl* II, *Br* I, *and Br* II, University of Maryland Technical Note BN-559, College Park, Maryland (1968).
[13] Hildum, J. S., and Cooper, J., Phys. Lett **A36,** 153 (1971).
[14] Kusch, H. J., Z. Astrophys. **67,** 64 (1967).
[15] Barnard, A. J., James, H. G., and Neufeld, C. R., Can. J. Phys. **46,** 1083 (1968).
[16] Konjevic, N., Platisa, M., and Puric, J., J. Phys. **B4,** 1541 (1971).
[17] Kusch, H. J., and Pritschow, H. P., Astron, Astrophys. **4,** 31 (1970).
[18] Heuschkel, J., and Kusch, H. J., Astron. Astrophys. **25,** 149 (1973).
[19] Jäger, H., Z. Phys. **223,** 19 (1969).
[20] Bogen, P., Z. Naturforsch. **A27,** 210 (1972).
[21] Hühn, R., and Kusch, H. J., Astron. Astrophys. **28,** 159 (1973).
[22] Helbig, V., and Kusch, H. J., Astron. Astrophys. **20,** 299 (1972).
[23] See, e.g., Wiese, W. L., "Electric Arcs," in *Methods of Experimental Physics*, Vol. 7B, B. Bederson and W. L. Fite, Editors, p. 307, Academic Press, New York (1968).
[24] Stokes, U. S., "Chemical Reactions in Plasma Jets," in *Reactions Under Plasma Conditions*, Vol. II, M. Venugopalan, Editor, p. 327, Wiley-Interscience, New York (1971).
[25] Griem, H. R., *Plasma Spectroscopy*, McGraw-Hill, New York (1964).
[26] Several chapters in *Plasma Diagnostics*, W. Lochte-Holtgreven, Editor, North-Holland, Amsterdam (1968).
[27] Chapelle, J., Sy, A., Cabannes, F., and Blandin, J., C.R.H. Acad. Sci. **B266,** 1513 (1968).
[28] Popenoe, C. H. and Shumaker, Jr., J. B., J. Res. Nat. Bur. Stand. (U.S.), **69A,** 495 (1965).
[29] Yamamoto, M., Phys. Rev. **146,** 137 (1966).
[30] Wiese, W. L., Kelleher, D. E., and Paquette, D. R., Phys. Rev. **A6,** 1132 (1972).
[31] Konjevic, N., and Roberts, J. R. (J. Phys. Chem. Ref. Data **5,** 201 (1976).
[32] Jaluška, N. W., and Craig, J. P., Phys. Rev. **A1,** 221 (1970).
[33] Kusch, H. J., Z. Astrophys. **67,** 64 (1967).
[34] King, P. G. R., and Stewart, J. G., New Scientist **17,** 180 (1963).
[35] Ashby, D. E. T. F., and Jephcott, D. F., Appl. Phys. Lett. **3,** 13 (1963).
[36] Gerardo, J. B., Verdeyen, J. T., and Gusinow, M. A., J. Appl. Phys. **36,** 2146 (1965).
[37] Gerardo, J. B., and Verdeyen, J. T., Appl. Phys. Lett. **3,** 121 (1963).
[38] Gerardo, J. B., and Verdeyen, J. T., Proc. IEEE **52,** 690 (1964).
[39] Hooper, E. B., and Bekefi, G., Appl. Phys. Lett. **7,** 133 (1965).
[40] Hooper, E. B., and Bekefi, G., Appl. Phys. **37,** 4083 (1966).
[41] Johnson, W. B., Larsen, A. B., and Sosnowski, T. P., Proc. VIIth Intl. Conf. on Phen. in Ion. Gases, Vol. III, B. Perovic and D. Tosic, Editors, Gradevinska Knjiga Publishers, Belgrade (1966).
[42] Verdeyen, J. T., Cherrington, B. E., and Fein, M. E., Appl. Phys. Lett. **5,** 360 (1966).
[43] Lin, C. S., Verdeyen, J. T., and Cherrington, B. E., Appl. Phys. **40,** 201 (1969).
[44] Wittemann, W. J., Appl. Phys. Lett. **10,** 347 (1967).
[45] Maignan, J., Fabre, E., and Vasseur, P., Phys. Lett. **A26,** 135 (1968).
[46] Konjevic, N., and Hearne, K. R., Phys. Lett. **A28,** 309 (1968).
[47] Alpher, R. A., and White, D. R., "Optical Interferometry," in *Plasma Diagnostic Techniques*, R. H. Huddlestone and S. L. Leonard, Editors, Academic Press, New York (1965).
[48] Martellucci, S., N.3-Supplemento at Nuovo Cimento, Series I, **5,** 642 (1967).
[49] Ascoli-Bartoli, V., "Plasma Diagnostics Based on Refractivity," in *Physics of Hot Plasmas*, B. J. Rye and J. C. Taylor, Editors, Oliver and Boyd, Edinburgh (1970).
[50] Alpher, R. A., and White, D. R., Phys. Fluids **2,** 162 (1959).
[51] Hearne, K. R., and Konjevic, N., Z. Phys. **204,** 443 (1967).
[52] Chapelle, J., Sy, A., Cabannes, F., and Blandin, J., J. Quant. Spectrosc. Radiat. Transfer **8,** 1201 (1968).
[53] Chapelle, J., and Sahal-Brechot, S., Astron. Astrophys **6,** 415 (1970).
[54] Murakawa, K., Phys. Rev. **146,** 135 (1966).
[55] Sanchez, A., Blaha, M., and Jones, W. W., Phys. Rev. **A8,** 774 (1973).
[56] Jalufka, N. W., Oertel, G. K., and Ofelt, G. S., Phys. Rev. Lett. **16,** 1073 (1966).
[57] Cooper, J., and Greig, J. R., J. Sci. Instrum. **40,** 433 (1963).
[58] Greig, J. R., and Cooper, J., Appl. Opt. **7,** 2166 (1968).
[59] Puric, J., Konjevic, N., Platisa, M., and Labat, J., Phys. Lett. **A37,** 425 (1971).
[60] Puric, J., and Konjevic, N., Z. Phys. **249,** 440 (1972).
[61] Roberts, D. E., and Barnard, A. J., J. Quant. Spectrosc. Radiat. Transfer **12,** 1205 (1972).
[62] Wiese, W. L., "Line Broadening," in *Plasma Diagnostic Techniques*, R. H. Huddlestone and S. L. Leonard, Editors, Academic Press, New York (1965).
[63] Roberts, D. E., J. Phys. **B1,** 53 (1968).
[64] Allen, A. W., Blaha, M., Jones, W. W., Sanchez, A., and Griem, H. R., Phys. Rev. **A11,** 477 (1975).
[65] Blandin, J., Sahal-Brechot, S., Chapelle, J., and Sy, A., Phys. Lett. **A26,** 487 (1968).
[66] Unsöld, A., *Physik der Sternatmosphaeren*, Springer Verlag, Berlin (1955).
[67] Lindholm, E., Ark. Math. Astron. Fys. **B28,** No. 3 (1941).
[68] Foley, H. M., Phys. Rev. **69,** 616 (1946).
[69] Allen, C. W., *Astrophysical Quantities*, 3rd Edition, Humanities Press, Inc., New Jersey (1974).
[70] Shore, B. W., and Menzel, D. H., *Principles of Atomic Spectra*, J. Wiley and Sons, New York (1968).
[71] Moore, C. E., *A Multiplet Table of Astrophysical Interest*, Nat. Bur. Stand. (U.S.), NSRDS-NBS 40 (1972); *An Ultraviolet Multiplet Table*, Nat. Bur. Stand. (U.S.), Circ. 488 (1950 and 1952); *Selected Tables of Atomic Spectra*, Nat. Bur. Stand. (U.S.), NSRDS-NBS 3, Secs. 1, 3, and 4, Government Printing Office, Washington, D.C. (1965, 1970, and 1971).
[72] Hadžomanolaković, D., Platisa, M., Konjevic, N., and Popovic, M., Z. Phys. **262,** 169 (1973).

[73] Sahal-Brechot, S., Astron. Astrophys. **2,** 322 (1969).
[74] Barnes, K. S., and Peach, G., J. Phys. **B3,** 350 (1970).
[75] Griem, H. R., Phys. Rev. **165,** 258 (1968).
[76] Bely, O., and Griem, H. R., Phys. Rev. **A1,** 97 (1970).
[77] Barnes, K. S., J. Phys. **B4,** 1377 (1971).
[78] Jones, W. W., private communication (1974).
[79] Roberts, J. R., and Eckerle, K. L., Phys. Rev. **159,** 104 (1967).
[80] Konjevic, N., Puric, J., Cirkovic, L. J., and Labat, J., J. Phys. **B3,** 999 (1970).
[81] Chapelle, J., and Czernichowski, A., Acta Phys. Pol. **A41,** 753 (1972).
[82] Bridges, J. M., and Wiese, W. L., Phys. Rev. **159,** 31 (1967).
[83] Kusch, H. J., and Oberschelp, E., Z. Astrophys. **67,** 85 (1967).
[84] Kusch, H. J., and Oberschelp, E., Z. Astrophys. **67,** 77 (1967).
[85] Morris, J. C., and Morris, R. V., Aerospace Research Laboratory Report No. ARL 70-0038 (1970).
[86] Jones, W. W., Phys. Rev. **A7,** 1826 (1973).
[87] Baur, J. F., and Cooper, J., to be published.
[88] Wiese, W. L., Smith, M. W., and Glennon, B. M., *Atomic Transition Probabilities*, Vol. I, NSRDS-NBS 4, U.S. Government Printing Office, Washington, D.C. (1966).
[89] Wiese, W. L., Smith, M. W., and Miles, B. M., *Atomic Transition Probabilities*, Vol. II, NSRDS-NBS 22, U.S. Government Printing Office, Washington, D.C. (1969).
[90] Miles, B. M., and Wiese, W. L., At. Data **1,** 1 (1969).
[91] Platisa, M., Popovic, M., and Konjevic, N., to be published in Astron. Astrophys.

6. Data Tables

6.1. Aluminum

Al II

Ground State	$1s^2 2s^2 2p^6 3s\ ^1S_0$
Ionization Potential	18.828 eV = 151860.4 cm^{-1}

The present situation on experimental Stark broadening data for Al II lines is quite unsatisfactory. One line was investigated with a gas driven shock tube [1] under very low instrumental resolution and another line was studied with an electromagnetically driven T-tube and a scanning Fabry-Perot interferometer [2]. Several more lines were measured with a pulsed, capillary discharge [3]. The electron density measurements of this experiment were based on previous results for the broadening of the C I 2478.6 Å line which are in strong disagreement with other experiments and with the theory [4].

References

[1] Miller, M. H., University of Maryland Tech. Note BN-550 (1968).
[2] Allen, A. W., Blaha, M., Jones, W. W., Sanchez, A., and Griem, H. R., Phys. Rev. **A11**, 477 (1975).
[3] Heuschkel, J., and Kusch, H. J., Astron. Astrophys. **25**, 149 (1973).
[4] Konjevic, N., and Roberts, J. R. (J. Phys. Chem. Ref. Data **5**, 201 (1976).

Key data on experiments

Ref.	Plasma source	Method of measurement		Remarks
		Electron density	Temperature	
[1]	Gas driven shock tube	H_β Stark width	Absolute intensity of Ne I 5852 Å line and H_β: line reversal technique applied to H_α	Photographic technique; low instrumental resolution (4 Å).
[2]	T-tube	Stark width of He I 3889 Å line	Ratio of He I 5016 Å line to adjacent continuum	No self-absorption check reported.
[3]	Pulsed capillary discharge	Stark width of C I 2479 Å line	Relative intensities of Mg II lines at 2791 Å and 2803 Å	Photographic technique; no self-absorption check reported.

Numerical results for Al II

Transition array	Multiplet (No.)	Wavelength Å	Temperature (K)	Electron density (cm^{-3})	w_m(Å)	w_m/w_{th}	d_m(Å)	d_m/d_{th}	Acc.	Ref.
1. $3s3p-3s(^2S)4s$	$^1P^o-^1S$ (7 UV)	2816.2	20 000	1.0×10^{17}	0.77		0.22		D	[3]
2. $3p^2-3s(^2S)4p$	$^1D-^1P^o$ (2)	4663.1	20 000	1.0×10^{17}	5.2	4.64			D	[3]
			18 500	1.0×10^{17}	0.90	0.80			B	[2]
3. $3p^2-3s(^2S)4f$	$^1D-^1F^o$ (11 UV)	2631.6	20 000	1.0×10^{17}	1.54		0.29		D	[3]
4. $3s3d-3s(^2S)4f$	$^3D-^3F^o$	3587	20 000	1.0×10^{17}	2.88				D	[3]
5. $3s4p-3s(^2S)5d$	$^1P^o-^1D$ (16)	5593.2	20 000	1.0×10^{17}	1.4				C	[1]

6.2. Argon

Ar II

Ground State $1s^2 2s^2 2p^6 3s^2 3p^5\ ^2P^o_{3/2}$

Ionization Potential $27.629\ eV = 222848.2\ cm^{-1}$

For Ar II by far the largest amount of material is available: a total of 33 papers were reviewed, of which 13 were selected [1–13].

In addition to the extensive number of Ar II shift and width data, several full line profiles were carefully investigated [7] and were found to be of Lorentzian shape. An example is presented in the general introduction (fig. 4). It is also worth mentioning that the temperature dependence of shift-to-width ratios has been experimentally studied [14, 15]. The wavelengths for all listed Ar II lines have been taken from the recent comprehensive description of the Ar II spectrum by Minnhagen [16].

References

[1] Popenoe, C. H., and Shumaker Jr., J. B., J. Res. Nat. Bur. Stand., Sect. **A69**, 495 (1965).

[2] Jalufka, N. W., Oertel, G. K., and Ofelt, G. S., Phys. Rev. Lett. **16**, 1073 (1966).

[3] Murakawa, K., Yamamoto, M., and Hashimoto, S., "Proceedings of the Seventh International Conference on Ionization Phenomena in Gases." Vol. II. 594 (Gradevinska Knjiga Publishing House, Belgrade (1966).

[4] Roberts, D. E., Phys. Lett. **22**, 417 (1966).

[5] Chapelle, J., Sy, A., Cabannes, F., and Blandin, J., J.Q.S.R.T. **8**, 1201 (1968): Chapelle, J., Sy, A., Cabannes, F., and Blandin, J., C.R.H. Acad. Sci., Ser. **B264**, 853 (1967).

[6] Blandin, J., Sahal-Brechot, S., Chapelle, J., and Sy, A., Phys. Lett. **26A**, 487 (1968).

[7] Chapelle, J., Sy, A., Cabannes, F., and Blandin, J., C.R.H. Acad. Sci., Ser. **B266**, 1513 (1968).

[8] Roberts, D. E., J. Phys. **B1**, 53 (1968).

[9] Powell, W. R., dissertation, Johns Hopkins University (1966), unpublished.

[10] Konjevic, N., Labat, J., Cirkovic, Lj., and Puric, J., Z. Phys. **235**, 35 (1970).

[11] Morris, J. C., and Morris, R. V., Aerospace Research Laboratories Report No. ARL 70–0038 (1970).

[12] Labat, J., Djenize, S., Cirkovic, Lj., and Puric, J., J. Phys. **B7**, 1174 (1974).

[13] Klein, L., J.Q.S.R.T. **13**, 567 (1973).

[14] Roberts, D. E., and Curzon, F. L., J. Phys. **B1**, 973 (1968).

[15] Chowdhury, S. S., J. Phys. **B2**, 1020 (1969).

[16] Minnhagen, L., Arkiv F. Fysik **25**, 203 (1964).

Key data on experiments

Ref.	Plasma source	Method of measurement		Remarks
		Electron density	Temperature	
[1]	Wall stabilized arc	H_β Stark width	Plasma composition data	
[2]	T-tube	Stark width of He I 5876 Å	Ratio of intensity of He I 5876 Å line to underlying continuum	No self-absorption check reported.
[3]	Plasma jet	Plasma composition data	Absolute intensity of Ar I 7940 Å line	No self-absorption check reported.
[4]	Z-pinch	Laser interferometer at 6328 Å	Intensity ratio of Ar II and Ar III lines	
[5]	Plasma jet	Plasma composition data	Absolute intensity of Ar I 4159 Å line and intensity of continuum	
[6]	Plasma jet	Plasma composition data	Absolute intensity of Ar I 4159 Å line and intensity of continuum	Shift measurements only.
[7]	Plasma jet	Plasma composition data	Absolute intensity of Ar I 4159 Å line and intensity of continuum	
[8]	Z-pinch	Laser interferometer at 6328 Å	Relative intensity of Ar II and Ar III lines	
[9]	T-tube	H_β and H_α Stark widths	Absolute intensities of Ar I and Ar II lines	Doppler broadening may be significant for some lines, but no correction is reported.
[10]	T-tube	Laser interferometer at 6328 Å, 1.15 μm and 3.39 μm	Boltzmann plot of Ar II line intensities	Doppler broadening is neglected.
[11]	Wall-stabilized pulsed arc	H_β Stark width	Absolute intensity of Ar I and Ar II lines	Shift measurements only, with photographic technique.

Key data on experiments—Continued

Ref.	Plasma source	Method of measurement		Remarks
		Electron density	Temperature	
[12]	T-tube	Laser interferometer	Boltzmann plot of Ar II line intensities	No self-absorption check reported. No discussion on Doppler and instrumental broadening.
[13]	Wall-stabilized arc	Plasma composition data	Ratio of Ar II 4348 Å to continuum at 4350 Å	

Numerical results for Ar II

Transition array	Multiplet (No.)	Wavelength Å	Temperature (K)	Electron density (cm^{-3})	w_m(Å)	w_m/w_{th}	d_m(Å)	d_m/d_{th}	Acc.	Ref.
1. $3p^4 3d$–$3p^4(^3P)4p$	^4D–$^4P^\circ$ (1)	4400.99	13 800	1.2×10^{17}	0.44	1.31			C	[5]
			13 800	1.0×10^{17}			0.050	0.55	B	[6]
			20 000	1.8×10^{17}			0.12	0.83	C	[11]
		4371.33	13 800	1.2×10^{17}	0.40	1.17			C	[5]
			13 800	1.0×10^{17}			0.060	0.67	B	[6]
			20 000	1.8×10^{17}			0.11	0.75	C	[11]
			16 500	1.0×10^{17}	0.30	1.07	0.07	0.88	C	[12]
		4332.03	20 000	1.8×10^{17}			0.11	0.75	C	[11]
		4431.00	13 800	1.2×10^{17}	0.40	1.17			C	[5]
			13 800	1.0×10^{17}			0.070	0.78	B	[6]
		4400.10	13 800	1.2×10^{17}	0.38	1.13			C	[5]
			13 800	1.0×10^{17}			0.050	0.55	B	[6]
			20 000	1.8×10^{17}			0.12	0.83	C	[11]
		4352.20	13 800	1.2×10^{17}	0.43	1.27			C	[5]
			13 800	1.0×10^{17}			0.050	0.55	B	[6]
			20 000	1.8×10^{17}			0.11	0.75	C	[11]
		4460.56	31 000	1.0×10^{17}	0.280	1.15			C+	[8]
		4420.91	20 000	1.8×10^{17}			0.11	0.75	C	[11]
	^4D–$^4D^\circ$ (2)	4013.86	13 800	1.2×10^{17}	0.40	1.47			C	[5]
			13 800	1.0×10^{17}			0.098	11.8	B	[6]
			31 000	1.0×10^{17}	0.316	1.76			C+	[8]
			20 000	1.8×10^{17}			0.044	0.59	C	[11]
			16 500	1.0×10^{17}	0.24	1.09	0.09	1.13	C	[12]
		3968.36	13 800	1.0×10^{17}			0.099	1.19	B	[6]
			20 000	1.8×10^{17}			0.08	0.59	C	[11]
		3914.77	20 000	1.8×10^{17}			0.06	0.45	C	[11]
		3944.27	20 000	1.8×10^{17}			0.09	0.68	C	[11]
		3875.26	20 000	1.8×10^{17}			0.05	0.38	C	[11]
		4038.81	20 000	1.8×10^{17}			0.08	0.59	C	[11]
		3992.05	20 000	1.8×10^{17}			0.08	0.59	C	[11]
	^4D–$^4S^\circ$ (5)	3499.48	20 000	1.8×10^{17}			0.10		C	[11]
2. $3p^4(^3P)3d$–$3p^4(^1D)4p'$	^2P–$^2D^\circ$ (30)	3605.88	20 000	1.8×10^{17}			0.07		C	[11]
	^2D–$^2D^\circ$ (39)	4481.81	8500–16 500	1.0×10^{17}	0.36–0.34				C+	[10]
			16 500	1.0×10^{17}	0.32		0.08		C	[12]
3. $3p^4 4s$–$3p^4(^3P)4p$	^4P–$^4P^\circ$ (6)	4806.02	11 800–13 000	(6.0–10.1) $\times10^{16}$	0.18–0.30	0.87–0.90	(−0.045)–(−0.075)	0.93–1.12	B	[1]
			18 000	1.03×10^{17}	0.39	1.07			C+	[2]
			31 000	4.4×10^{17}	1.78	1.18			C	[4]
			13 800	1.2×10^{17}	0.43	0.92			C	[5]
			13 800	1.0×10^{17}			−0.090	1.45	B	[6]
			13 000	1.0×10^{17}	0.36	0.91			B	[7]

Numerical results for Ar II – Continued

Transition array	Multiplet (No.)	Wavelength Å	Temperature (K)	Electron density (cm^{-3})	w_m(Å)	w_m/w_{th}	d_m(Å)	d_m/d_{th}	Acc.	Ref.
			31 000	1.0×10^{17}	0.404	1.19			C+	[8]
			13 900	8.0×10^{16}	0.22	0.71	−0.054	1.11	C	[9]
			9700–16 500	1.0×10^{17}	0.32–0.30	0.73–0.80			C+	[10]
			20 000	1.8×10^{17}			−0.06	1.57	C	[11]
			16 500	1.0×10^{17}	0.32	0.84	−0.08	2.0	C	[12]
		4933.21	31 000	1.0×10^{17}	0.428	1.26			C+	[8]
			16 500	1.0×10^{17}	0.34	0.89	−0.08	2.0	C	[12]
		4735.91	18 000	1.0×10^{17}	0.39	1.07			C+	[2]
			13 900	8.0×10^{16}	0.22	0.71	−0.061	1.24	C	[9]
			8500–16 500	1.0×10^{17}	0.34–0.30	0.74–0.80			C+	[10]
			20 000	1.8×10^{17}			−0.08	2.09	C	[11]
			16 500	1.0×10^{17}	0.32	0.84	−0.10	2.5	C	[12]
		4847.82	13 800	1.2×10^{17}	0.45	0.97			C	[5]
			13 800	1.0×10^{17}			−0.087	1.40	B	[6]
			13 000	1.0×10^{17}	0.36	0.91			B	[7]
			31 000	1.0×10^{17}	0.376	1.11			C+	[8]
			8500–16 500	1.0×10^{17}	0.34–0.30	0.74–0.80			C+	[10]
			20 000	1.8×10^{17}			−0.08	2.09	C	[11]
			16 500	1.0×10^{17}	0.32	0.84	−0.08	2.0	C	[12]
		5009.33	13 800	1.0×10^{17}			−0.090	1.45	B	[6]
			16 500	1.0×10^{17}	0.34	0.89	−0.08	2.0	C	[12]
		5062.04	31 000	4.4×10^{17}	1.94	1.29			C	[4]
			31 000	1.0×10^{17}	0.44	1.29			C+	[8]
	^4P–$^4D^\circ$ (7)	4348.06	14 500–15 600	$(1.0–1.8)\times10^{17}$	0.135–0.183	0.47–0.74	(−0.17)–(−0.40)	0.36–0.55	C	[3]
			13 800	1.2×10^{17}	0.40	1.08			C	[5]
			13 800	1.0×10^{17}			−0.050	0.98	B	[6]
			13 000	1.0×10^{17}	0.32	1.02			B	[7]
			31 000	1.0×10^{17}	0.230	0.83			C+	[8]
			13 900	8.0×10^{16}	0.20	0.82	−0.025	0.61	C	[9]
			9700–16 500	1.0×10^{17}	0.36–0.32	1.01–1.11			C+	[10]
			20 000	1.8×10^{17}			−0.07	2.29	C	[11]
			16 500	1.0×10^{17}	0.26	0.87	−0.06	1.50	C	[12]
			11 950–13 500	$(0.63–1.28)\times10^{17}$	0.142–0.290	0.68–0.73			C+	[13]
		4426.01	18 000	1.0×10^{17}	0.35	1.30			C+	[2]
			13 800	1.2×10^{17}	0.40	1.08			C	[5]
			13 800	1.0×10^{17}			−0.055	1.08	B	[6]
			13 000	1.0×10^{17}	0.32	1.02			B	[7]
			13 900	8.0×10^{16}	0.20	0.82			C	[9]
			20 000	1.8×10^{17}			−0.06	1.94	C	[11]
			16 500	1.0×10^{17}	0.24	0.80	−0.06	1.5	C	[12]
		4430.19	13 800	1.2×10^{17}	0.40	1.08			C	[5]
			13 800	1.0×10^{17}			−0.058	1.14	B	[6]
			16 500	1.0×10^{17}	0.24	0.80	−0.08	2.0	C	[12]
		4266.53	31 000	4.4×10^{17}	1.48	1.01			C	[4]
			31 000	1.0×10^{17}	0.336	1.21			C+	[8]
			20 000	1.8×10^{17}			−0.06	1.94	C	[11]
			16 500	1.0×10^{17}	0.28	0.93	−0.07	1.8	C	[12]
		4331.20	13 800	1.2×10^{17}	0.395	1.08			C	[5]
			13 800	1.0×10^{17}			−0.042	0.82	B	[6]
			13 000	1.0×10^{17}	0.32	1.02			B	[7]
			20 000	1.8×10^{17}			−0.05	1.65	C	[11]
		4379.67	13 800	1.2×10^{17}	0.39	1.05			C	[5]
			13 800	1.0×10^{17}			−0.044	0.86	B	[6]
			13 000	1.0×10^{17}	0.32	1.02			B	[7]
			9700–16 500	1.0×10^{17}	0.34–0.32	0.95–1.11			C+	[10]
			16 500	1.0×10^{17}	0.30	1.0	−0.08	2.0	C	[12]

Numerical results for Ar II—Continued

Transition array	Multiplet (No.)	Wavelength Å	Temperature (K)	Electron density (cm^{-3})	w_m(Å)	w_m/w_{th}	d_m(Å)	d_m/d_{th}	Acc.	Ref.
		4178.37	20 000	1.8×10^{17}			−0.05	1.65	C	[11]
		4282.90	20 000	1.8×10^{17}			−0.06	1.94	C	[11]
	$^4P-^2D^\circ$	4082.39	20 000	1.8×10^{17}			0.07		C	[11]
	(8)	4228.16	13 800	1.2×10^{17}	0.435				C	[5]
			13 800	1.0×10^{17}			−0.01		D	[6]
	$^4P-^4S^\circ$	3729.31	18 000	1.0×10^{17}	1.1	5.0			D	[2]
	(10)		8500–16 500	1.0×10^{17}	0.26–0.24	0.92–1.07			C+	[10]
			20 000	1.8×10^{17}			−0.06	(*)	C	[11]
			16 500	1.0×10^{17}	0.26	1.08	0.08	1.00	C	[12]
		3850.58	13 800	1.2×10^{17}	0.33	1.19			C	[5]
			13 800	1.0×10^{17}			−0.001	(*)	C	[6]
			13 000	1.0×10^{17}	0.26	1.08			B	[7]
			31 000	1.0×10^{17}	0.320	1.58			C+	[8]
			20 000	1.8×10^{17}			−0.09	(*)	C	[11]
		3928.63	13 800	1.2×10^{17}	0.33	1.19			C	[5]
			13 800	1.0×10^{17}			−0.001	(*)	C	[6]
			13 000	1.0×10^{17}	0.26	1.08			B	[7]
	$^2P-^4D^\circ$	5145.32	8500–16 500	1.0×10^{17}	0.44–0.36				C+	[10]
	(13)		16 500	1.0×10^{17}	0.36		0.05		C	[12]
	$^2P-^2P^\circ$	4879.86	31 000	4.4×10^{17}	2.16	1.26			C	[4]
	(14)		31 000	1.0×10^{17}	0.492	1.26			C-	[8]
			13 900	8.0×10^{16}	0.36	1.00	−0.031	0.23	C	[9]
			9700–16 500	1.0×10^{17}	0.44–0.40	0.87–0.94			C+	[10]
			20 000	1.8×10^{17}			−0.10	0.38	C	[11]
			16 500	1.0×10^{17}	0.42	0.95	−0.05	0.31	C	[12]
		4726.86	13 800	1.2×10^{17}	0.48	0.89			C	[5]
			13 800	1.0×10^{17}			−0.078	0.47	B	[6]
			8500–16 500	1.0×10^{17}	0.42–0.36	0.79–0.85			C+	[10]
			20 000	1.8×10^{17}			−0.08	0.30	C	[11]
			16 500	1.0×10^{17}	0.36	0.82	−0.08	0.5	C	[12]
	$^2P-^2P^\circ$	4545.05	13 800	1.2×10^{17}	0.50				C	[5]
	(15)		13 800	1.0×10^{17}			−0.052		B	[6]
			13 000	1.0×10^{17}	0.38				B	[7]
			8500–16 500	1.0×10^{17}	0.32–0.32				C+	[10]
			20 000	1.8×10^{17}			−0.05		C	[11]
			16 500	1.0×10^{17}	0.32		0.08		C	[12]
		4657.89	13 800	1.2×10^{17}	0.475				C	[5]
			13 800	1.0×10^{17}			−0.055		B	[6]
			13 000	1.0×10^{17}	0.38				B	[7]
			8500–16 500	1.0×10^{17}	0.30–0.28				C+	[10]
			20 000	1.8×10^{17}			−0.03		C	[11]
			16 500	1.0×10^{17}	0.32		0.08		C	[12]
		4764.86	13 800	1.2×10^{17}	0.505				C	[5]
			13 800	1.0×10^{17}			−0.052		B	[6]
			8500–16 500	1.0×10^{17}	0.32–0.30				C+	[10]
			20 000	1.8×10^{17}			−0.05		C	[11]
			16 500	1.0×10^{17}	0.32		0.10		C	[12]
	$^2P-^2S^\circ$	4375.95	20 000	1.8×10^{17}			0.0			[11]
	(17)	4579.35	13 800	1.2×10^{17}	0.42				C	[5]
			13 800	1.0×10^{17}			−0.029		B	[6]

Numerical results for Ar II—Continued

Transition array	Multiplet (No.)	Wavelength Å	Temperature (K)	Electron density (cm^{-3})	w_m(Å)	w_m/w_{th}	d_m(Å)	d_m/d_{th}	Acc.	Ref.
			9700–16 500	1.0×10^{17}	0.46–0.42				C	[10]
			20 000	1.8×10^{17}			0.0			[11]
			16 500	1.0×10^{17}	0.32		0.0		C	[12]
4. $3p^44s$–$3p^4(^1D)4p'$	^2P–$^2P^\circ$	2942.89	20 000	1.8×10^{17}			0.21		C	[11]
	^2P–$^2D^\circ$	2844.13	20 000	1.8×10^{17}			−0.04		C	[11]
	(16 UV)	2847.82	20 000	1.8×10^{17}			−0.03		C	[11]
5. $3p^44s'$–$3p^4(^1D)4p'$	^2D–$^2F^\circ$	4609.56	13 800	1.2×10^{17}	0.47				C	[5]
	(31)		13 800	1.0×10^{17}			−0.048		B	[6]
			13 000	1.0×10^{17}	0.365				B	[7]
			13 900	8.0×10^{16}	0.22				C	[9]
			9700–16 500	1.0×10^{17}	0.34–0.32				C	[10]
			20 000	1.8×10^{17}			0.0			[11]
			16 500	1.0×10^{17}	0.34		−0.05		C	[12]
		4589.90	13 800	1.2×10^{17}	0.44				C	[5]
			13 800	1.0×10^{17}			−0.047		B	[6]
			13 000	1.0×10^{17}	0.365				B	[7]
			20 000	1.8×10^{17}			0.00			[11]
	^2D–$^2P^\circ$	4277.52	20 000	1.8×10^{17}			0.28		C	[11]
	(32)	4237.22	20 000	1.8×10^{17}			0.28		C	[11]
	^2P–$^2D^\circ$	4079.58	20 000	1.8×10^{17}			−0.08		C	[11]
	(33)	4042.90	16 500	1.0×10^{17}	0.22				C	[12]
6. $3p^44p$–$3p^4(^3P)4d$	$^4P^\circ$–^4D	3514.39	20 000	1.8×10^{17}			0.43		C	[11]
	(44)	3535.32	20 000	1.8×10^{17}			0.45		C	[11]
		3509.78	20 000	1.8×10^{17}			0.39		C	[11]
		3454.10	20 000	1.8×10^{17}			0.40		C	[11]
	$^4D^\circ$–^4D	3780.84	20 000	1.8×10^{17}			0.45		C	[11]
	(54)	3826.81	20 000	1.8×10^{17}			0.39		C	[11]
		3872.14	20 000	1.8×10^{17}			0.39		C	[11]
		3880.34	20 000	1.8×10^{17}			0.34		C	[11]
		3763.50	20 000	1.8×10^{17}			0.48		C	[11]
		3799.38	20 000	1.8×10^{17}			0.37		C	[11]
		3841.52	20 000	1.8×10^{17}			0.33		C	[11]
		3900.62	20 000	1.8×10^{17}			0.45		C	[11]
		3911.57	20 000	1.8×10^{17}			0.44		C	[11]
	$^4D^\circ$–^4F	3520.00	20 000	1.8×10^{17}			0.43		C	[11]
	(56)	3548.52	20 000	1.8×10^{17}			0.50		C	[11]
	$^4D^\circ$–^4P	3370.93	20.000	1.8×10^{17}			0.41		C	[11]
	(57)	3421.62	20 000	1.8×10^{17}			0.45		C	[11]
		3565.03	20 000	1.8×10^{17}			0.54		C	[11]
		3480.51	20 000	1.8×10^{17}			0.45		C	[11]
	$^4D^\circ$–^2F	3397.90	20 000	1.8×10^{17}			0.50		C	[11]
	(59)	3430.42	20 000	1.8×10^{17}			0.41		C	[11]
	$^2D^\circ$–^4D	3988.16	20 000	1.8×10^{17}			0.40		C	[11]
	(65)									
	$^2D^\circ$–^2F	3464.13	20 000	1.8×10^{17}			0.50		C	[11]
	(70)									
	$^2D^\circ$–^2P	3137.63	20 000	1.8×10^{17}			0.38		C	[11]
	(71)									

Numerical results for Ar II—Continued

Transition array	Multiplet (No.)	Wavelength Å	Temperature (K)	Electron density (cm^{-3})	w_m(A)	w_m/w_{th}	d_m(A)	d_m/d_{th}	Acc.	Ref.
	$^2P^o$–^2P	3293.64	20 000	1.8×10^{17}			0.55		C+	[11]
	(83)	3307.29	20 000	1.8×10^{17}			0.67		C+	[11]
		3366.59	20 000	1.8×10^{17}			0.52		C+	[11]
	$^4S^o$–^4P	3868.52	20 000	1.8×10^{17}			0.60		C+	[11]
	(90)	3932.55	20 000	1.8×10^{17}			0.56		C+	[11]
		3979.36	20 000	1.8×10^{17}			0.63		C+	[11]
	$^2S^o$–^2P	3388.53	20 000	1.8×10^{17}			0.43		C	[11]
	(96)									
7. $3p^44p'$–$3p^4(^1D)4d'$	^2F–$^2D^o$	3414.46	20 000	1.8×10^{17}			0.78		C+	[11]
	(107)									
	$^2F^o$–^2F	3376.44	20 000	1.8×10^{17}			0.66		C+	[11]
	(109)	3350.93	31 000	4.4×10^{17}	2.60				C	[4]
			31 000	1.0×10^{17}	0.592				C+	[8]
			20 000	1.8×10^{17}			0.53		C+	[11]
		3365.54	20 000	1.8×10^{17}			0.62		C+	[11]
	$^2P^o$–^2D	3660.44	20 000	1.8×10^{17}			0.49		C	[11]
	(116)	3639.83	20 000	1.8×10^{17}			0.45		C	[11]
	$^2D^o$–^2D	3803.17	20 000	1.8×10^{17}			0.62		C+	[11]
	(129)									
	$^2D^o$–^2F	3737.89	20 000	1.8×10^{17}			0.68		C+	[11]
	(131)	3718.21	20 000	1.8×10^{17}			0.64		C+	[11]
		3724.52	20 000	1.8×10^{17}			0.59		C+	[11]
8. $3p^14p$–$3p^4(^3P)5s$	$^4P^o$–^4P	3720.43	20 000	1.8×10^{17}			0.60		C+	[11]
	(42)	3669.61	20 000	1.8×10^{17}			0.76		C+	[11]
		3678.27	20 000	1.8×10^{17}			0.63		C+	[11]
		3622.14	20 000	1.8×10^{17}			0.59		C+	[11]
		3809.46	20 000	1.8×10^{17}			0.57		C+	[11]
		3770.52	20 000	1.8×10^{17}			0.50		C+	[11]
	$^4P^o$–^2P	3650.89	20 000	1.8×10^{17}			0.64		C+	[11]
	(43)									
	$^2D^o$–^2P	4033.82	20 000	1.8×10^{17}			0.68		C+	[11]
	(52)	4179.30	20 000	1.8×10^{17}			0.66		C+	[11]
		4156.09	20 000	1.8×10^{17}			0.72		C+	[11]
	$^2D^o$–^2P	4218.67	20 000	1.8×10^{17}			0.78		C+	[11]
	(64)									
	$^2P^o$–^2P	4222.64	20 000	1.8×10^{17}			0.70		C+	[11]
	(77)	4129.69	20 000	1.8×10^{17}			0.68		C+	[11]
9. $3p^14p$–$3p^4(^1D)5s'$	$^2P^o$–^2D	2806.17	20 000	1.8×10^{17}			0.32		C	[11]
	(17 UV)									
10. $3p^14p'$–$3p^4(^1D)5s'$	$^2F^o$–^2D	3946.10	20 000	1.8×10^{17}			0.66		C+	[11]
	(105)	3925.72	20 000	1.8×10^{17}			0.68		C+	[11]
11. $3d'^2F$–$(^3P_2)4f[4]^o$		3046.08	20 000	1.8×10^{17}			0.23		C	[11]
		3066.89	20 000	1.8×10^{17}			0.21		C	[11]
12. d'^2D–$(^1D)4f[3]^o$		2708.27	20 000	1.8×10^{17}			0.14		C	[11]
		2744.80	20 000	1.8×10^{17}			0.18		C	[11]
13. d'^2D–$(^1D)4f[2]$		2732.50	20 000	1.8×10^{17}			0.31		C	[11]
		2769.75	20 000	1.8×10^{17}			0.27		C	[11]

Numerical results for Ar II—Continued

Transition array	Multiplet (No.)	Wavelength Å	Temperature (K)	Electron density (cm^{-3})	w_m(Å)	w_m/w_{th}	d_m(Å)	d_m/d_{th}	Acc.	Ref.
14. $3d'^2P-(^1D)4f[2]^\circ$		2931.48	20 000	1.8×10^{17}			0.23		C	[11]
15. $3d'^2P-(^1D)4f[1]^\circ$		2960.26	20 000	1.8×10^{17}			0.12		C	[11]

(*) Theory predicts opposite sign.

Ar III

Ground State $1s^2 2s^2 2p^6 3s^2 3p^4\ ^3P_2$

Ionization Potential 40.74eV = 328600 cm^{-1}

In the only experimental investigation [1] of Ar III Stark widths, comparisons are made with the semiclassical calculations by Cooper and Oertel[2]. The agreement with the hyperbolic path approximation is fairly satisfactory.

References

[1] Platisa, M., Popovic, M., Dimitrijevic, M., and Konjevic, N., Z. Naturforsch. **30a**, 212 (1975).
[2] Cooper, J., and Oertel, G. N., Phys. Rev. **180**, 286 (1969).

Key data on experiments

Ref.	Plasma source	Method of measurement		Remarks
		Electron density	Temperature	
[1]	Low pressure pulsed arc	Laser interferometry at 6328 Å	Boltzmann plot of Ar II line intensities	

Numerical results for Ar III

Transition array	Multiplet (No.)	Wavelength Å	Temperature (K)	Electron density (cm^{-3})	w_m(Å)	w_m/w_{th}	d_m(Å)	d_m/d_{th}	Acc.	Ref.
1. $3d^3 3d''-3p^3(^2P^\circ)4p''$	$^3P^\circ-^3P$ (6)	3391.8	21 100	4.4×10^{16}	0.058				C+	[1]
2. $3p^3 4s-3p^3(^4S^\circ)4p$	$^5S^\circ-^5P$ (1)	3285.8	21 100–23 080	$(4.4-8.0)\times10^{16}$	0.064–0.082				C+	[1]
		3301.9	21 100–23 080	$(4.4-8.0)\times10^{16}$	0.061–0.077				C+	[1]
3. $3p^3 4s'-3p^3(^2D^\circ)4p'$	$^3D^\circ-^3D$ (2)	3480.6	21 100–23 080	$(4.4-8.0)\times10^{16}$	0.058–0.081				C+	[1]
	$^3D^\circ-^3F$ (3)	3336.1	21 100–23 080	$(4.4-8.0)\times10^{16}$	0.064–0.083				C+	[1]

Ar IV

Ground State $1s^2 2s^2 2p^6 3s^2 3p^3\ {}^4S^\circ_{3/2}$

Ionization Potential 59.81 eV = 482400 cm^{-1}

In the only experimental investigation [1] of Ar IV Stark widths, comparisons are made with the semiclassical calculations by Cooper and Oertel [2]. The agreement with the hyperbolic path approximation is fairly satisfactory.

References

[1] Platisa, M., Popovic, M., Dimitrijevic, M., and Konjevic, N., Z. Naturforsch. **30a**, 212 (1975).
[2] Cooper, J., and Oertel, G. N., Phys. Rev. **180**, 286 (1969).

Key data on Experiments

Ref.	Plasma source	Method of measurement: Electron density	Method of measurement: Temperature	Remarks
[1]	Low-pressure pulsed arc	Laser interferometry at 6328 Å	Boltzmann plot of Ar II line intensities	

Numerical results for Ar IV

Transition array	Multiplet (No.)	Wavelength Å	Temperature (K)	Electron Density (cm^{-3})	w_m(Å)	w_m/w_{th}	d_m(Å)	d_m/d_{th}	Acc.	Ref.
1. $3p^2 4s - 3p^2(^3P)4p$	$^4P - ^4D^\circ$ (4 UV)	2809.4	20 750–22 200	$(3.8–5.6) \times 10^{16}$	0.023–0.033				C	[1]
	$^4P - ^4D^\circ$ (5 UV)	2640.3	20 750–22 200	$(3.8–5.6) \times 10^{16}$	0.021–0.031				C	[1]

6.3. Barium

Ba II

Ground State $1s^2 2s^2 2p^6 3s^2 3p^6 3d^{10} 4s^2 4p^6 4d^{10} 5s^2 5p^6 6s\ {}^2S_{1/2}$

Ionization Potential 10.004 eV = 80686.87 cm^{-1}

A fairly large number of experimental data is available for this ion, and strong discrepancies are encountered between the results of refs. [1] and [3]. Self-absorption effects may be partly to blame for this, since the tests of optical depth carried out for the inhomogeneous plasma source of ref. [1] appear to be questionable. Theoretical comparison data have been calculated by W. W. Jones [4] on the basis of the semiclassical theory [5, 6]. Ref. [3] supersedes the similar work of ref. [7].

References

[1] Jaeger, H., Z. Phys. **223**, 19 (1969).
[2] Puric, J., and Konjevic, N., Z. Phys. **249**, 440 (1972).
[3] Hadziomerspahic, D., Platisa, M., Konjevic, N., and Popovic, M., Z. Phys. **262**, 169 (1973).
[4] Jones, W. W., private communication (1975).
[5] Jones, W. W., Benett, S. M., and Griem, H. R., Tech. Report No. 71–128, University of Maryland, College Park, Md. (1971).
[6] Griem, H. R., *Spectral Line Broadening by Plasmas*, Academic Press, New York (1974).
[7] Platisa, M., Puric, J., Konjevic, N., and Labat, J., Astron. Astrophys. **15**, 325 (1971).

Key data on experiments

Ref.	Plasma source	Method of measurement		Remarks
		Electron density	Temperature	
[1]	Discharge sliding along the surface of liquid jet	H_β Stark width	Boltzmann plot of Ba II line intensities	Photographic technique; self-absorption checks on indirectly derived (Abel inverted) data
[2]	T-tube	Laser interferometry at 6328 Å	Boltzmann plot of Ar II line intensities	Shift measurements only.
[3]	Z-pinch	Laser interferometry at 6328 Å	Boltzmann plot of Ar II line intensities	

Numerical results for Ba II

Transition array	Multiplet (No.)	Wavelength Å	Temperature (K)	Electron density (cm^{-3})	w_m(Å)	w_m/w_{th}	d_m(Å)	d_m/d_{th}	Acc.	Ref.
1. $5d-(^1S)6p$	$^2D-^2P^o$	6141.7	13 200	1.0×10^{17}	1.58	2.19			D	[1]
	(2)		16 800	1.0×10^{17}			0.07	(*)	C	[2]
			27 100	1.0×10^{17}	0.28	0.45			C	[3]
			31 700	1.0×10^{17}	0.28	0.46			C+	[3]
		6496.9	16 800	1.0×10^{17}			0.07	(*)	C	[2]
			27 100	1.0×10^{17}	0.28	0.45	0.05	(*)	C+	[3]
			31 700	1.0×10^{17}	0.28	0.46			C+	[3]
		5853.7	13 200	1.0×10^{17}	1.32	1.83			D	[1]
2. $6s-(^1S)6p$	$^2S-^2P^o$	4554.0	13 200	1.0×10^{17}	0.80	1.81			D	[1]
	(1)		16 800	1.0×10^{17}			−0.06	0.36	C	[2]
			27 100	1.0×10^{17}	0.26	0.67			C+	[3]
			31 700	1.0×10^{17}	0.24	0.62	−0.07	0.48	C+	[3]
		4934.1	13 200	1.0×10^{17}	0.94	2.12			D	[1]
			16 800	1.0×10^{17}			−0.06	0.36	C	[2]
			27 100	1.0×10^{17}	0.24	0.62			C+	[3]
3. $6p-(^1S)6d$	$^2P^o-^2D$	4130.6	13 200	1.0×10^{17}	1.24	0.90			D	[1]
	(4)	4166.0	13 200	1.0×10^{17}	1.26	0.91			D	[1]
		3891.8	16 800	1.0×10^{17}			0.26	0.39	C+	[2]
			31 700	1.0×10^{17}	0.28		0.33	0.57	C+	[3]
4. $6p-(^1S)7s$	$^2P^o-^2S$	4899.9	13 200	1.0×10^{17}	1.48				D	[1]
	(3)	4524.9	13 200	1.0×10^{17}	1.28				D	[1]

* Theory predicts opposite sign.

6.4. Beryllium

Be II

Ground State $1s^22s\ ^2S_{1/2}$

Ionization Potential 18.211 eV = 146882.86 cm^{-1}

The three selected experimental papers deal with investigations of the broadening and shift of the resonance doublet [1–3]. The mutual agreement of the data for these two very narrow lines (< 0.1 Å in the reported range of electron densities) is well within the limits of claimed experimental error. The line profiles are most precisely measured by the authors of ref. [3], who employ a scanning Fabry-Perot interferometer. Therefore these results may be considered slightly more accurate than the others. However, no check for self-absorption effects is noted in this paper and figure 2 of ref. [3] indicates a deviation in the doublet intensity ratio which may be due to the presence of some self-absorption.

References

[1] Puric, J., and Konjevic, N., Z. Phys. **249**, 440 (1972).
[2] Hadziomerspahic, D., Platisa, M., Konjevic, N., and Popovic, M., Z. Phys. **262**, 169 (1973).
[3] Sanchez, A., Blaha, M., and Jones, W. W., Phys. Rev. **A8**, 774 (1973).

Key data on experiments

Ref.	Plasma Source	Method of measurement		Remarks
		Electron density	Temperature	
[1]	T-tube	Laser interferometry at 6328 Å	Boltzmann plot of Ar II line intensities	Shift measurements only.
[2]	Z-pinch	Laser interferometry at at 6328 Å	Boltzmann plot of Ar II line intensities	
[3]	T-tube	He I 3889 Å Stark width	Ratio of intensity of He I 5016 to continuum	No self-absorption check reported.

Numerical results for Be II

Transition array	Multiplet (No.)	Wavelength Å	Temperature (K)	Electron density (cm^{-3})	w_m(Å)	w_m/w_{th}	d_m(Å)	d_m/d_{th}	Acc.	Ref.
1. $2s-2p$	$^2S-^2P^o$ (1)	3130.4	16 800	1.0×10^{17}			−0.03	0.80	C	[1]
			34 800	1.0×10^{17}	0.04	0.57	−0.04	1.41	C	[2]
			19 000	1.0×10^{17}	0.070	0.82			C+	[3]
		3131.1	16 800	1.0×10^{17}			−0.03	0.80	C	[1]
			34 800	1.0×10^{17}	0.06	0.86	−0.03	1.03	C	[2]
			19 000	1.0×10^{17}	0.070	0.82			C+	[3]

6.5. Cadmium

Cd II

Ground State $1s^22s^22p^63s^23p^63d^{10}4s^24p^64d^{10}5s\ ^2S_{1/2}$

Ionization Potential 16.908 eV = 136374.74 cm^{-1}

Only one experimental paper is available on the investigation of the broadening of single ionized cadmium lines [1]. Considering the high-density conditions and rather large dimensions of the employed pulsed discharge, self-absorption could be significant, but no check of it is reported.

References

[1] Kusch, H. J., and Oberschelp, E., Z. Astrophys. **67**, 85 (1967).

Key data on experiments

Ref.	Plasma source	Method of measurement		Remarks
		Electron density	Temperature	
[1]	Pulsed discharge	H_β Stark width	Plasma composition data	Photographic technique; no self-absorption check reported.

Numerical results for Cd II

Transition array	Multiplet (No.)	Wavelength Å	Temperature (K)	Electron density (cm^{-3})	w_m(Å)	w_m/w_{th}	d_m(Å)	d_m/d_{th}	Acc.	Ref.
1. $4d5s-4d(^1S)5p$	$^2S-^2P^o$ (1)	2265.0	11 100	1.0×10^{17}	1.93				D	[1]
2. $4d5p-4d(^1S)5s$	$^2P^o-^2D$	3250.3	11 100	1.0×10^{17}	0.53				D	[1]
3. $4d5p-4d(^1S)6s$	$^2P^o-^2S$ (6)	2572.9	11 100	1.0×10^{17}	0.48				D	[1]
4. $4d5p-4d(^1S)5d$	$^2P^o-^2D$ (7)	2312.8	11 100	1.0×10^{17}	0.53				D	[1]
		2321.1	11 100	1.0×10^{17}	0.50				D	[1]
		2194.6	11 100	1.0×10^{17}	0.88				D	[1]
5. $4d5d-4d(^1S)4f$	$^2D-^2F^o$	5378.1	11 100	1.0×10^{17}	5.77				D	[1]
		5337.5	11 100	1.0×10^{17}	4.40				D	[1]

6.6. Calcium

Ca II

Ground State $1s^22s^22p^63s^23p^64s\ ^2S_{1/2}$

Ionization Potential 11.871 eV = 95751.87 cm^{-1}

A large number of experimental papers deal with the broadening of singly ionized calcium lines from which 11 have been selected [1–11]. Many of them are devoted to the investigation of the principal resonance lines. It is seen that large discrepancies still exist. A graphical comparison of the data is presented in figure 11 of the general discussion.

The very large width values (normalized to $N_e = 10^{17}$ cm^{-3}) of ref. [4] may be traced to the special diagnostic method applied by these authors. The electron density determination is based on a Stark width for the C I 2478 Å line, which had been determined earlier by one of the authors experimentally and which is apparently wrong, disagreeing with fairly reliable theoretical data by a factor of 6. A likely cause of the disagreement is self-absorption effects, according to a recent review[12].

References

[1] Yamamoto, M., Phys. Rev. **146,** 137 (1966).
[2] Roberts, J. R., and Eckerle, K. L., Phys. Rev. **159,** 104 (1967).
[3] Chapelle, J., and Sahal-Brechot, S., Astron. Astrophys. **6,** 415 (1970).
[4] Kusch, H. J., and Pritschow, H. P., Astron. Astrophys. **4,** 31 (1970).
[5] Hildum, J. S., and Cooper, J., Phys. Lett. **A36,** 153 (1971).
[6] Jones, W. W., Sanchez, A., Greig, J. R., and Griem, H. R., Phys. Rev. **A5,** 2318 (1972).
[7] Puric, J., and Konjevic, N., Z. Phys. **249,** 440 (1972).
[8] Roberts, D. E., and Barnard, A. J., J.Q.S.R.T. **12,** 1205 (1972).
[9] Hadziomerspahic, D., Platisa, M., Konjevic, N., and Popovic, M., Z. Phys. **262,** 169 (1973).
[10] Hühn, R., and Kusch, H. J., Astron. Astrophys. **28,** 159 (1973).
[11] Baur, J. F., and Cooper, J., to be published.
[12] Konjevic, N., and Roberts, J. R., to be published in J. Chem. Phys. Ref. Data.

Key data on experiments

Ref.	Plasma source	Method of measurement		Remarks
		Electron density	Temperature	
[1]	Plasma jet	H_β Stark width	Absolute intensity of H_β	Side on observations; inhomogeneity of plasma only approximately taken into account
[2]	T-tube	H_β Stark width	Estimated from previous experiment	No Doppler correction reported.
[3]	Plasma jet	Plasma composition data	Absolute intensity of recombination continuum and Brem-strahlung coefficient at 4000 Å	

Key data on experiments—Continued

Ref.	Plasma source	Method of measurement		Remarks
		Electron density	Temperature	
[4]	Pulsed capillary discharge	Stark width of C I 2478 Å	Relative intensities of Mg II lines	No self-absorption check reported; photographic technique.
[5]	Parallel-rail shock-tube	Michelson interferometer illuminated at 6328 Å	Relative intensities of Ar II lines	No corrections for Doppler and instrumental broadening reported.
[6]	T-tube	Stark width of He I 3889 Å	Ratio of intensities of He I 5015.7 Å line to continuum	No self-absorption check reported.
[7]	T-tube	Laser interferometry at 6328 Å	Boltzmann plot of Ar II line intensities	Shift measurements only.
[8]	Low pressure pulsed arc	Laser interferometry at 6328 Å	Relative intensities of Ar II lines	Data are only given graphically.
[9]	Z-pinch	Laser interferometry at 6328 Å	Boltzmann plot of Ar II line intensities	
[10]	Gas-stabilized arc	Shift of Ar I 4159 Å line; plasma composition data; absolute intensity of continuum	Absolute intensity of Ar I 4159 Å line and intensity ratio of Ca I/Ca II lines	
[11]	Gas driven shock tube	Laser interferometry at 6328 Å and 1.15 μm; Stark width of H_α	Line reversal technique	

Numerical results for Ca II

Transition array	Multiplet (No.)	Wavelength Å	Temperature (K)	Electron density (cm^{-3})	w_m(Å)	w_m/w_{th}	d_m(Å)	d_m/d_{th}	Acc.	Ref.
1. $3d-4p$	$^2D-^2P^o$ (2)	8542.1	12 000	6.9×10^{16}	0.23	0.26			B	[3]
2. $4s-4p$	$^2S-^2P^o$ (1)	3933.7	11 400–11 600	$(4.0-6.4)\times10^{16}$	0.039–0.079	0.33–0.43	0.0046–0.0155	0.09–0.19	D	[1]
			30 000	2.35×10^{17}	0.24	0.47			C	[2]
			12 000	7.6×10^{16}	0.15	0.71			B	[3]
			17 500	1.0×10^{18}	10.0	3.95			D	[4]
			19 000	1.0×10^{17}	0.172	0.69			B	[6]
			14 200	1.0×10^{17}			−0.09	0.71	C	[7]
			16 000–28 000	1.0×10^{17}	0.16–0.25	0.62–1.07	(−0.01)–(−0.04)	0.09–0.35	C	[8]
			25 100–29 200	1.0×10^{17}	0.22–0.18*	0.92–0.78	(−0.06)–(−0.05)	0.60–0.52	C	[9]
		3968.5	17 500	1.0×10^{18}	10.3	4.07			D	[4]
			18 560	1.0×10^{17}	0.188	0.75			B	[5]
			14 200	1.0×10^{17}			−0.09	0.71	C	[7]
			16 000–28 000	1.0×10^{17}	0.16–0.25	0.62–1.07	(−0.01)–(−0.04)	0.09–0.35	C	[8]
			25 100	1.0×10^{17}	0.20*	0.84	−0.06	0.60	C	[9]
			29 200	1.0×10^{17}			−0.06	0.62	C	[9]
			7 500	1.0×10^{17}	0.174	0.53			B	[11]
3. $4p-5s$	$^2P^o-^2S$ (3)	3706.3	17 500	1.0×10^{18}	13.7	2.24	3.3	1.03	D	[4]
			14 200	1.0×10^{17}			0.17	0.50	C+	[7]
			25 100	1.0×10^{17}			0.17	0.57	C+	[7]
			10 000	1.0×10^{17}	0.70	1.01	0.238	0.65	C	[10]

Numerical results for Ca II – Continued

Transition array	Multiplet (No.)	Wavelength Å	Temperature (K)	Electron density (cm^{-3})	w_m(Å)	w_m/w_{th}	d_m(Å)	d_m/d_{th}	Acc.	Ref.
		3736.9	7 500	1.0×10^{18}	18.2	2.98	4.16	1.3	D	[4]
			14 200	1.0×10^{17}			0.18	0.53	C+	[7]
			25 100	1.0×10^{17}	0.30*	0.53	0.16	0.53	C+	[9]
			10 000	1.0×10^{17}	0.69	1.00	0.186	0.51	C	[10]
4. $4p$–$4d$	$^2P^o$–^2D	3158.9	14 200	1.0×10^{17}			0.18	0.73	C+	[7]
	(4)		25 100–29 200	1.0×10^{17}	0.32–0.30*	0.74–0.71	0.15–0.15	0.70–0.72	C+	[9]

*Accuracies of the Stark widths are B.

6.7. Carbon

C II

Ground State $1s^22s^22p\ ^2P^o_{1/2}$

Ionization Potential 24.383 eV = 196664.7 cm^{-1}

Two experiments on C II Stark broadening parameters are selected [1, 2], which have both been performed with pulsed plasma sources. Most of the results are estimated to be of low accuracy so that new experiments are very desirable.

One might also mention the experiment by Fortna et al. [3] on the resonance lines, performed with a T-type electromagnetically driven shock tube. This work had to be done under conditions where the line centers are optically thick. Thus only an indirect determination of the line widths could be obtained by computing profiles of various Stark widths and using the equation of radiative transfer to achieve the best fit with the observed profiles. The best agreement was obtained with a width which corresponded exactly to that computed from theory.

References

[1] Kusch, H. J., Z. Astrophys. **67**, 64 (1967).
[2] Roberts, J. R., and Eckerle, K. L., Phys. Rev. **159**, 104 (1967).
[3] Fortna, J. D. E., Elton, R. C., and Griem, H. R., Phys. Rev. **A2**, 1150 (1970).

Key data on experiments

Ref.	Plasma source	Method of measurement		Remarks
		Electron density	Temperature	
[1]	Pulsed discharge	H_β Stark width	Plasma composition	Photographic technique; no self-absorption check reported.
[2]	T-tube	Stark width of He I 3889 Å	Estimated from comparison with previous experiment	

Numerical results for C II

Transition array	Multiplet (No.)	Wavelength Å	Temperature (K)	Electron density (cm^{-3})	w_m(Å)	w_m/w_{th}	d_m(Å)	d_m/d_{th}	Acc.	Ref.
1. $2s2p^2$–$2p^3$	^2P–$^2D^o$	2509.1	12 800	1.0×10^{17}	0.34				D	[1]
	(14 UV)	2511.7	12 800	1.0×10^{17}	0.34				D	[1]
		2512.0	12 800	1.0×10^{17}	0.34				D	[1]
2. $2s^22p^2$–$2s^2(^1S)3p$	^2S–$^2P^o$	2836.7	12 800	1.0×10^{17}	1.07	6.28			D	[1]
	(13 UV)	2837.6	12 800	1.0×10^{17}	1.07	6.28			D	[1]
3. $3p$–$(^1S)4s$	$^2P^o$–^2S	3920.7	12 800	1.0×10^{17}	0.82	0.78			D	[1]
	(4)		30 000	$(1.4–1.5)\times10^{17}$	1.44–1.52	1.11–1.08			C	[2]
		3919.0	12 800	1.0×10^{17}	0.82	0.78			D	[1]
4. $3p$–$(^1S)4d$	$^2P^o$–^2D	2746.5	12 800	1.0×10^{17}	1.82	1.82			D	[1]
	(15 UV)	2747.3	12 800	1.0×10^{17}	1.82	1.82			D	[1]

Numerical results for C II – Continued

Transition array	Multiplet (No.)	Wavelength Å	Temperature (K)	Electron density (cm^{-3})	w_m(Å)	w_m/w_{th}	d_m(Å)	d_m/d_{th}	Acc.	Ref.
5. $3d$–(^{1}S)$4f$	^{2}D–^{2}F°	4267.2	12 800	1.0×10^{17}	2.20	1.18			D	[1]
	(6)	4267.0	12 000–13 500	$(0.5–4.0)\times10^{17}$	1.1–8.7	1.14–1.18			D	[1]
6. $2s2p3d$–$2s2p(^3P°)4f$	^{4}D°–^{4}F	4074.5	12 800	1.0×10^{17}	2.11				D	[1]
	(36)	4074.9	12 800	1.0×10^{17}	2.11				D	[1]
		4076.0	12 800	1.0×10^{17}	2.11				D	[1]
7. $3d$–(^{1}S)$5p$	^{2}D–^{2}P°	3361.1	30 000	$(1.4–1.5)\times10^{17}$	1.76–2.52	0.68–0.90			C	[2]
	(7)									
8. $3d$–(^{1}S)$5f$	^{2}D–^{2}F°	2992.6	12 800	1.0×10^{17}	4.01	0.95			D	[1]
	(8)		30 000	$(1.4–1.5)\times10^{17}$	7.58–7.34	1.54–1.40			C	[2]

C III

Ground State $1s^22s^2\ ^1S_0$

Ionization Potential 47.887 eV = 386241.0 cm^{-1}

There is no overlap between the experimental data of Kusch[1] and Bogen[2], and no semiclassical calculations exist for comparison. Bogen has compared his data with the semiempirical Gaunt-factor approximation [3] and finds good agreement for transitions to principal quantum numbers $n=4$ and 5, but discrepancies by factors of 2 and more for the transitions within the $n=3$ shell.

References

[1] Kusch, N. J., Z. Astrophys. **67**, 64 (1967).
[2] Bogen, P., Z. Naturforschg **27A**, 210 (1972).
[3] Griem, H. R., Phys. Rev. **165**, 258 (1968).

Key data on experiments

Ref.	Plasma source	Method of measurement		Remarks
		Electron density	Temperature	
[1]	Pulsed discharge	Stark width of H_β	Plasma composition data	Photographic technique; no check for self-absorption reported.
[2]	Theta-pinch	Stark width of He II 3203 Å	Absolute line intensities and Fowler-Milne method	No corrections for instrumental and Doppler broadening reported.

Numerical results for C III

Transition array	Multiplet (No.)	Wavelength Å	Temperature (K)	Electron density (cm^{-3})	w_m(Å)	w_m/w_{th}	d_m(Å)	d_m/d_{th}	Acc.	Ref.
1. $2s2p$–$2p^2$	^{1}P°–^{1}D	2296.9	12 800	1.0×10^{17}	0.34				D	[1]
	(8 UV)									
2. $2s3s$–$2s(^2S)3p$	^{3}S–^{3}P°	4647.4	60 000	4×10^{17}	0.95				D	[2]
	(1)									
3. $2s3p$–$2s(^2S)3d$	^{1}P°–^{1}D	5696.0	60 000	4×10^{17}	1.9				C	[2]
	(2)									
4. $2s3p$–$2s(^2S)4d$	^{1}P°–^{1}D	1531.8	60 000	4×10^{17}	0.43				D	[2]
5. $2s3d$–$2s(^2S)4f$	^{1}D–^{1}F°	2162.9	60 000	4×10^{17}	0.46				D	[2]
6. $2s4p$–$2s(^2S)5d$	^{3}P°–^{3}D	3609.3	60 000	4×10^{17}	6.2				C	[2]
	(10)									
7. $2s4f$–$2s(^2S)5g$	^{1}F°–^{1}G	4187.0	60 000	4×10^{17}	4.1				C	[2]
	(18)									

C IV

Ground State $1s^2 2s\ ^2S_{1/2}$

Ionization Potential 64.492 eV = 520178.4 cm^{-1}

The data obtained by Bogen [1] with a theta-pinch are the only available source. No semiclassical calculations exist for comparison, but good agreement is obtained with the semiempirical Gaunt-factor approximation [2].

References

[1] Bogen, P., Z. Naturforsch. **27a**, 210 (1972).
[2] Griem, H. R., Phys. Rev. **165**, 258 (1968).

Key data on experiments

Ref.	Plasma source	Method of measurement		Remarks
		Electron density	Temperature	
[1]	Theta pinch	Stark width of He II 3203 Å	Absolute line intensities and Fowler-Milne method	No corrections for instrumental and Doppler broadening reported.

Numerical results for C IV

Transition array	Multiplet (No.)	Wavelength Å	Temperature (K)	Electron density (cm^{-3})	w_m(Å)	w_m/w_{th}	d_m(Å)	d_m/d_{th}	Acc.	Ref.
1. $2s$–$2p$	^2S–$^2P^o$	1548.2	60 000	4×10^{17}	0.024				D	[1]
	(1 UV)	1550.8	60000	4×10^{17}	0.024				D	[1]
2. $3s$–$3p$	^2S–$^2P^o$	5801.5	60 000	4×10^{17}	1.6				C	[1]
	(1)	5818.1	60000	4×10^{17}	1.6				C	[1]

6.8. Chlorine

Cl II

Ground State $1s^2 2s^2 2p^6 3s^2 3p^4\ ^3P_2$

Ionization Potential 23.81 eV = 192070 cm^{-1}

A large number of Stark broadening data for singly ionized chlorine lines were obtained with an electromagnetically driven T-tube [1], from low-pressure pulsed arc experiments [2, 3] and with a gas driven shock tube [4]. The good agreement between the sets of experimental data from [1] and [2, 3] is quite encouraging since they were obtained in different plasma sources where the electron densities differed by almost an order of magnitude.

Unfortunately, mainly due to the incompleteness of atomic energy level data for Cl II, there are only few theoretical data [5] to compare with these experiments.

References

[1] Konjevic, N., Radivojevic, D., Cirkovic, Lj., and Labat, J., J. Phys. **B3**, 1742 (1970).
[2] Konjevic, N., Platisa, M., and Puric, J., J. Phys. **B4**, 1541 (1971).
[3] Puric, J., Konjevic, N., Platisa, M., and Labat, J., Phys. Lett. **A37**, 425 (1971).
[4] Bengtson, R. D., Maryland University Tech. Note BN-559 (1968).
[5] Griem, H. R., *Spectral Line Broadening by Plasmas*, Academic Press, New York (1974) p. 211.

Key data on experiments

Ref.	Plasma source	Method of measurement		Remarks
		Electron density	Temperature	
[1]	T-tube	Laser interferometry at 6328 Å and 1.15 μm	Boltzmann plot of intensities of Cl II lines	
[2, 3]	Low pressure pulsed arc	Laser interferometry at 6328 Å	Boltzmann plot of intensities of Cl II lines	
[4]	Gas driven shock tube	H_β Stark width; plasma composition data	Absolute intensity of Ne I 5852 line; line reversal technique H_α central intensity	Photographic technique; low spectral resolution (2 and 4 Å).

Numerical results for Cl II

Transition array	Multiplet (No.)	Wavelength Å	Temperature (K)	Electron density (cm^{-3})	w_m(Å)	w_m/w_{th}	d_m(Å)	d_m/d_{th}	Acc.	Ref.
1. $3p^3 3d$– $3p^3(^4S°)4p$	$^5D°$–^5P (2)	5443.4	18 600	6.8×10^{16}	0.33		1.09		B	[2]
2. $3p^3 3d''$– $3p^3(^2P°)4p''$	$^1P°$–^1D (47)	4943.2	14 500–18 600	$(5.0-6.8) \times 10^{16}$	0.19–0.26				B	[2]
			18 600	6.8×10^{16}			0.05		C	[3]
	$^1D°$–^1P (51)	4740.4	14 500–18 600	$(5.0-6.8) \times 10^{16}$	0.33–0.45				B	[2]
			18 600	6.8×10^{16}			0.00			[3]
3. $3p^3 4s$– $3p^3(^4S°)4p$	$^5S°$–^5P (1)	4810.1	13 300–17 800	$(2.64-4.27) \times 10^{17}$	1.21–1.71	1.00–0.92			C	[1]
			18 600	6.8×10^{16}	0.26	0.88	0.00	(*)	B	[2], [3]
			11 500	1.0×10^{17}	0.90	1.87			D	[4]
		4819.5	13 300–17 800	$(2.64-4.27) \times 10^{17}$	1.16–1.79	0.95–0.97			C	[1]
			18 600	6.8×10^{16}	0.27	0.93	0.00	(*)	B	[2], [3]
		4794.5	13 300–17 800	$(2.64-4.27) \times 10^{17}$	1.16–1.71	0.92–0.98			C	[1]
			18 600	6.8×10^{16}	0.29	0.98	0.00	(*)	B	[2], [3]
			11 500	1.0×10^{17}	0.81	1.69			D	[4]
	$^3S°$–^3P (3)	5221.3	18 600	6.8×10^{16}	0.31	0.83	0.00	(**)	B	[2], [3]
4. $3p^3 4s'$– $3p^3(^2D°)4p'$	$^3D°$–^3D (16)	5078.2	14 700–17 800	$(3.72-4.27) \times 10^{17}$	2.16–3.39				C	[1]
			14 500–18 600	$(5.0-6.8) \times 10^{16}$	0.28–9.34				B	[2]
			18 600	6.8×10^{16}			0.00			[3]
	$^3D°$–^3F (17)	4896.8	13 300–17 800	$(2.64-4.27) \times 10^{17}$	1.32–2.05				C	[1]
			14 500–18 600	$(5.0-6.8) \times 10^{16}$	0.25–0.31				B	[2]
			18 600	6.8×10^{16}			−0.08		C	[3]
		4917.7	14 700–17 800	$(3.72-4.27) \times 10^{17}$	1.93–2.14				C	[1]
			18 600	6.8×10^{16}			−0.10		C+	[3]
		4904.8	14 700–17 800	$(3.72-4.27) \times 10^{17}$	1.86–2.14				C	[1]
			18 600	6.8×10^{16}			−0.12		C+	[3]
	$^3D°$–^3P (19)	4291.8	14 500–18 600	$(5.0-6.8) \times 10^{16}$	0.22–0.26				B	[2]
			18 600	6.8×10^{16}			0.08		C	[3]
		4304.1	14 500–18 600	$(5.0-6.8) \times 10^{16}$	0.21–0.26				B	[2]
			18 600	6.8×10^{16}			0.12		C+	[3]
		4336.3	14 500–18 600	$(5.0-6.8) \times 10^{16}$	0.22–0.24				B	[2]
			18 600	6.8×10^{16}			0.09		C	[3]
		4343.6	14 500–18 600	$(5.0-6.8) \times 10^{16}$	0.23–0.26				B	[2]
			18 600	6.8×10^{16}			0.08		C	[3]
	$^1D°$–^1D (29)	4132.5	18 600	6.8×10^{16}	0.30		0.08		B	[2], [3]
5. $3p^3 4s''$– $3p^3(^2P°)4p''$	$^3P°$–^3D (40)	4785.4	14 500–18 600	$(5.0-6.8) \times 10^{16}$	0.21–0.24				B	[2]
			18 600	6.8×10^{16}			0.00			[3]
		4768.7	14 500–18 600	$(5.0-6.8) \times 10^{16}$	0.21–0.24				B	[2]
			18 600	6.8×10^{16}			0.00			[3]
		4778.9	14 500–18 600	$(5.0-6.8) \times 10^{16}$	0.18–0.23				B	[2]
			18 600	6.8×10^{16}			0.05		C	[3]
6. $3p^3 4s''$–$3p^4 4s$	$^3P°$–^3P (41)	4490.0	14 500–18 600	$(5.0-6.8) \times 10^{16}$	0.33–0.44				B	[2]
			18 600	6.8×10^{16}			0.06		C	[3]
		4504.3	14 500–18 600	$(5.0-6.8) \times 10^{16}$	0.30–0.39				B	[2]
			18 600	6.8×10^{16}			0.10		C+	[3]
		4536.8	18 600	6.8×10^{16}	0.42				B	[2]
7. $3p^3 4p$– $3p^3(^2D°)3d'$	^3P–$^3P°$ (32)	5285.5	18 600	6.8×10^{16}	0.30		0.10		B	[2], [3]

Numerical results for Cl II—Continued

Transition array	Multiplet (No.)	Wavelength Å	Temperature (K)	Electron density (cm^{-3})	w_m(Å)	w_m/w_{th}	d_m(Å)	d_m/d_{th}	Acc.	Ref.
	$^3P-^3D^\circ$ (33)	5173.1	18 600	6.8×10^{16}	0.31		0.04		B	[2], [3]
8. $3p^34p'-3p^3(^2D^\circ)4d'$	$^3F-^3F^\circ$ (68)	3913.9	14 500–18 600	$(5.0-6.8)\times 10^{16}$	0.27–0.35				B	[2]
			18 600	6.8×10^{16}			0.14		C+	[3]
		3916.7	14 500–18 600	$(5.0-6.8)\times 10^{16}$	0.27–0.34				B	[2]
			18 600	6.8×10^{16}			0.19		C+	[3]
		3917.6	18 600	6.8×10^{16}	0.34		0.19		B	[2], [3]
	$^3F-^3G^\circ$ (69)	3820.2	14 500–18 600	$(5.0-6.8)\times 10^{16}$	0.28–0.31				B	[2]
			18 600	6.8×10^{16}			*0.13*		C+	*[3]*
		3827.2	14 500–18 600	$(5.0-6.8)\times 10^{16}$	0.26–0.31				B	[2]
			18 600	6.8×10^{16}			0.07		C	[3]
		3833.4	14 500–18 600	$(5.0-6.8)\times 10^{16}$	0.28–0.34				B	[2]
			18 600	6.8×10^{16}			0.12		C+	[3]
9. $3p^34p-3p^3(^4S^\circ)5s$	$^5P-^5S^\circ$ (24)	4241.4	14 500–18 600	$(5.0-6.8)\times 10^{16}$	0.29–0.35				B	[2]
			18 600	6.8×10^{16}			*0.14*		C+	*[3]*
		4253.5	14 500–18 600	$(5.0-6.8)\times 10^{16}$	0.32–0.37				B	[2]
10. $3p^34p'-3p^3(^2P^\circ)5s'$	$^3D-^3D^\circ$ (60)	4147.1	14 500–18 600	$(5.0-6.8)\times 10^{16}$	0.33–0.45				B	[2]
			18 600	6.8×10^{16}			*0.17*		C+	*[3]*
	$^3F-^3D^\circ$ (66)	4270.6	18 600	6.8×10^{16}	0.39		0.19		C+	[2], [3]
		4276.5	14 500–18 600	$(5.0-6.8)\times 10^{16}$	0.32–0.33				B	[2]
			18 600	6.8×10^{16}			0.17		C+	[3]

(*) Theory predicts negative shift.
(**) Accuracy estimate applies to width only.

6.9. Germanium

Ge II

Ground State $1s^22s^22p^63s^23p^63d^{10}4s^24p\ ^2P^\circ_{1/2}$

Ionization Potential 15.934 eV = 128521.3 cm^{-1}

The only available data are from a recent experiment with a gas-driven shock tube [1]. For the strong disagreement between theory and experiment on the multiplet $5s\,^2S-5p\,^2P$ several possible explanations have been advanced. Wrong energy assignments for the perturbing atomic levels appear to be a rather likely cause.

References

[1] Jones, W. W., and Miller, M. H., Phys. Rev. **A10**, 1803 (1974).

Key data on experiments

Ref.	Plasma source	Method of measurement: Electron density	Method of measurement: Temperature	Remarks
[1]	Gas-driven-shock tube	H_β Stark width	Absolute intensity of Ne I 6402 Å line and H_α line reversal technique applied to H_α	Photographic technique.

Numerical results for Ge II

Transition array	Multiplet (No.)	Wavelength Å	Temperature (K)	Electron density (cm^{-3})	w_m(Å)	w_m/w_{th}	d_m(Å)	d_m/d_{th}	Acc.	Ref.
1. $4s^25s-4s^2(^1S)5p$	$^2S-^2P^\circ$ (1)	5893.4	11 000	1.0×10^{17}	2.61	2.14			B	[1]
		6021.0	11 000	1.0×10^{17}	1.64	1.34			B	[1]
2. $4s^25p-4s^2(^1S)5d$	$^2P^\circ-^2D$ (2)	4815.6	11 000	1.0×10^{17}	3.10	1.02			B	[1]
		4741.8	11 000	1.0×10^{17}	2.75	0.91			B	[1]
		4824.1	11 000	1.0×10^{17}	3.10	1.02			B	[1]
3. $4s^24d-4s^2(^1S)4f$	$^2D-^2F^\circ$	5131.8	11 000	1.0×10^{17}	2.27	0.96			B	[1]
		5178.5	11 000	1.0×10^{17}	2.42	1.04			B	[1]
		5178.6	11 000	1.0×10^{17}	2.42	1.04			B	[1]

6.10. Magnesium

Mg II

Ground State $1s^22s^22p^63s\ ^2S_{1/2}$

Ionization Potential 15.035 eV = 121267.61 cm^{-1}

Five different plasma sources were used for the investigation of broadening parameters of Mg II lines: a plasma jet [1], electromagnetically driven T-tubes [2, 3], a low-pressure pulsed arc [4], a stabilized arc [5] and a Z-pinch [6]. With the exception of the result for the width of the resonance line 2801.7 Å reported in ref. 4, the agreement among the experiments and with the theory is well within the limits of experimental and theoretical uncertainty estimates.

References

[1] Chapelle, J., and Sahal-Brechot, S., Astron. Astrophys. **6**, 415 (1970).
[2] Jones, W. W., Sanchez, A., Greig, J. R., and Griem, H. R., Phys. Rev. **A5**, 2318 (1972).
[3] Puric, J., and Konjevic, N., Z. Phys. **249**, 440 (1972).
[4] Roberts, D. E., and Barnard, A. J., J.Q.S.R.T. **12**, 1205 (1972).
[5] Helbig, V., and Kusch, H. J., Astron. Astrophys. **20**, 299 (1972).
[6] Hadziomerspahic, D., Platisa, M., Konjevic, N., and Popovic, M., Z. Phys. **262**, 169 (1973).

Key data on experiments

Ref.	Plasma source	Method of measurement		Remarks
		Electron density	Temperature	
[1]	Plasma jet	Plasma composition data	Absolute intensity of Ar continuum at 4000 Å	Photographic technique.
[2]	T-tube	Comparison with analogous experiment on Ca II.	Ratio of intensities of He I 5015.7 Å line to continuum	No self-absorption check reported.
[3]	T tube	Laser interferometry at 6328 Å	Boltzmann plot of Ar II line intensities	(Shift measurements only.)
[4]	Low-pressure pulsed arc	Laser interferometry at 6328 Å	Relative intensities of Mg II lines	
[5]	Gas stabilized high pressure arc	Shift of Ar I 4158 Å line, absolute intensity of Mg I and Mg II lines and of Ar I continuum at 3600 Å	Absolute intensity of Ar I 4158.6 Å line and Mg I/Mg II line intensities	Photographic technique; no self-absorption check reported.
[6]	Z-pinch	Laser interferometry at 6328 Å	Boltzmann plot of Ar II line intensities	

Numerical results for Mg II

Transition	Multiplet (No.)	Wavelength Å	Temperature (K)	Electron density (cm^{-3})	w_m(Å)	w_m/w_{th}	d_m(Å)	d_m/d_{th}	Acc.	Ref.
1. $3s$–$3p$	^2S–$^2P^\circ$	2802.7	12000	9.0×10^{16}	0.11	1.20			C	[1]
	(1 UV)		18500	1.0×10^{17}	0.088	1.00			C+	[2]
			14000–21000	1.0×10^{17}	0.050–0.047	0.51–0.47	0.05–0.06	(*)	C	[4]
			31700–34800	1.0×10^{17}	0.08 –0.08	1.04–1.05			C	[6]
		2795.5	31700	1.0×10^{17}	0.08	1.04			C	[6]
			34800	1.0×10^{17}	0.06	0.79	0.01(**)	(*)	C	[6]
2. $3p$–$4s$	$^2P^\circ$–^2S	2928.6	16800	1.0×10^{17}			0.08	0.56	C	[3]
	(2 UV)		10000	1.0×10^{17}	0.35	1.10	0.06	0.36	C	[5]
		2936.5	16800	1.0×10^{17}			0.08	0.56	C	[3]
			10000	1.0×10^{17}	0.36	1.13	0.08	0.49	C	[5]
3. $3d$–$4f$	^2D–$^2F^\circ$	4481.2	12000	1.0×10^{17}	2.1	0.82			C+	[1]
	(4)		10000	1.0×10^{17}	2.13	0.78	0.32	(*)	C+	[5]

*Theory predicts negative shift.
**Accuracy of shift data "D".

6.11. Mercury

Hg II

Ground State $1s^22s^22p^63s^23p^63d^{10}4s^24p^64d^{10}4f^{14}5s^25p^65d^{10}6s\ ^2S_{1/2}$

Ionization Potential 18.756 eV = 151280 cm^{-1}

A high-current mercury arc was used as a plasma source in side-on observations of the Stark width of a single mercury line [1]. A rather low accuracy for the result is indicated, since the line width and electron density are not measured precisely and neither the radial inhomogeneity of the source nor any self-absorption checks are discussed. There are no theoretical data available for comparison.

Reference

[1] Murakawa, K., Phys. Rev. **146**, 135 (1966).

Key data on experiments

Ref.	Plasma source	Method of measurement		Remarks
		Electron density	Temperature	
[1]	High-current mercury arc	Inglis-Teller formula	Profile of strongly self-absorbed line (Göing method)	No self-absorption check reported. No allowance made for inhomogeneity of source.

Numerical results for Hg II

Transition array	Multiplet (No.)	Wavelength Å	Temperature (K)	Electron density (cm^{-3})	w_m(Å)	w_m/w_{th}	d_m(Å)	d_m/d_{th}	Acc.	Ref.
1. $5d^96s^2$–$5d^{10}(^1S)6p$	^2D–$^2P^\circ$	3984.0	6500	2.6×10^{16}	0.06*		0.08*		D	[1]

6.12. Nitrogen

N II

Ground State $1s^2 2s^2 2p^2\ ^3P_0$

Ionization Potential 29.601 eV = 238750.5 cm^{-1}

Four of the selected experiments on N II lines were performed in electromagnetically driven T-tubes [1–4] and one with a low-pressure pulsed arc [5]. In general, the results of these experiments agree well with each other, with the exception of the data from ref. [1]. As suggested later by one of the authors [6], undetected inhomogeneities in their T-tube plasma are most probably the cause of this discrepancy. The electron densities in ref. [1] should probably all be multiplied by about a factor of two [6] which greatly decreases the degree of the discrepancy with the other experiments.

An additional recent Stark broadening experiment has been carried out by Fortna et al. [7] on the resonance lines, also with a T-tube. This work was done under conditions where the line centers were optically thick. Thus only an indirect determination of the line widths could be obtained by computing profiles with various Stark widths and using the equation of radiative transfer to achieve the best fit with the observed profiles. The best fit was obtained with a width 50 percent greater than that expected from theory.

References

[1] Day, R. A., and Griem, H. R., Phys. Rev. **140**, A1129 (1965).
[2] Berg, H. F., Ervens, W., and Furch, B., Z. Phys. **206**, 309 (1967).
[3] Jalufka, N. W., and Craig, J. P., Phys. Rev. **A1**, 221 (1970).
[4] Konjevic, N., Mitrovic, V., Cirkovic, Lj., and Labat, J., Fizika **2**, 129 (1970).
[5] Popovic, M., Platisa, M., and Konjevic, N., Astron. Astrophys. **41**, 463 (1975).
[6] Griem, H. R., *Spectral Line Broadening by Plasmas*, Academic Press, New York 1974, p. 204.
[7] Fortna, J. D. E., Elton, R. C., and Griem, H. R., Phys. Rev. **A2**, 1150 (1970).

Key data on experiments

Ref.	Plasma source	Method of measurement		Remarks
		Electron density	Temperature	
[1]	T-tube	Stark width of He I 3889 Å	Plasma composition data and absolute intensities of N II lines	See introductory remarks.
[2]	T-tube	Stark width of He I 3889 Å	Relative intensities of He I and N II lines	
[3]	T-tube	Stark width of He I 3889 Å	Absolute intensity of N II 4631 Å line	Doppler broadening, not reported, sometimes significant.
[4]	T-tube	Laser interferometry at 6328 Å	Boltzmann plot of N II line intensities	No self-absorption check reported.
[5]	Low-pressure pulsed arc	Laser interferometry at 6328 Å	Boltzmann plot of N II line intensities	

Numerical results for N II

Transition array	Multiplet (No.)	Wavelength Å	Temperature (K)	Electron density (cm^{-3})	w_m(Å)	w_m/w_{th}	d_m(Å)	d_m/d_{th}	Acc.	Ref.
1. $2p3s$–$2p(^2P^\circ)3p$	$^3P^\circ$–^3P (5)	4613.9	18 800	6.3×10^{17}	0.9	0.41	0.5	0.61	D	[1]
			22 000	1.0×10^{17}	0.40	1.18			C	[2]
			22 800	1.0×10^{17}	0.35	1.03			C+	[3]
			23 150	4.8×10^{16}	0.16	0.99			B	[5]
		4630.5	22 000	1.0×10^{17}	0.40	1.18			C	[2]
			22 800	1.0×10^{17}	0.35	1.03			C+	[3]
			16 200	3.12×10^{17}	0.87	0.79			C	[4]
			23 150	4.8×10^{16}	0.16	0.99			B	[5]
		4643.1	22 800	1.0×10^{17}	0.35	1.03			C+	[3]
		4621.1	23 150	4.8×10^{16}	0.15	0.94			B	[5]

Numerical results for N II—Continued

Transition array	Multiplet (No.)	Wavelength Å	Temperature (K)	Electron density (cm^{-3})	w_m(Å)	w_m/w_{th}	d_m(Å)	d_m/d_{th}	Acc.	Ref.
	$^3P^\circ$–^1D (6)	3955.8	23 150	4.8×10^{16}	0.14				B	[5]
	$^1P^\circ$–^3P (11)	4654.6	16 200	3.12×10^{17}	0.87				C	[4]
	$^1P^\circ$–^1D (12)	3995.0	22 000	1.0×10^{17}	0.34				C	[2]
			22 800	1.0×10^{17}	0.30				C+	[3]
			16 200–18 300	$(3.12–4.84) \times 10^{17}$	0.87–1.45				C	[4]
			23 150	4.8×10^{16}	0.15				B	[5]
2. $2p3p$–$2p(^2P^\circ)3d$	^1P–$^3F^\circ$ (14)	3564.8	16 200	3.12×10^{17}	0.94				C	[4]
	^1P–$^1D^\circ$ (15)	4447.0	22 000	1.0×10^{17}	0.45				C	[2]
			22 800	1.0×10^{17}	0.28				C+	[3]
			23 150	4.8×10^{16}	0.15				B	[5]
	^3D–$^3D^\circ$ (20)	4803.3	23 150	4.8×10^{16}	0.16	0.92			B	[5]
	^3P–$^3P^\circ$ (29)	5495.7	18 800	6.3×10^{17}	1.2	0.38	0.5	0.41	D	[1]
			22 800	1.0×10^{17}	0.58	1.19			C+	[3]
3. $2p3p$–$2p(^2P^\circ)4s$	^1P–$^1P^\circ$ (18)	3006.9	19 600	3.3×10^{17}	0.9	0.66	0.6	0.91	D	[1]
			18 800	6.3×10^{17}	1.65	0.63	1.1	0.86	D	[1]
			22 800	1.0×10^{17}	0.60	1.45			C	[2]
			23 150	4.8×10^{16}	0.22	1.12			B	[5]
	^3P–$^3P^\circ$ (30)	3838.4	19 600	3.3×10^{17}	1.9	0.76	0.9	0.91	D	[1]
			22 000	1.0×10^{17}	0.87	1.14	0.8	2.86	C	[2]
			22 800	1.0×10^{17}	1.0	1.32			C+	[3]
4. $2p3d$–$2p(^2P^\circ)4f$	$^3F^\circ$–^3G (39)	4041.3	23 150	4.8×10^{16}	0.40				B	[5]
	$^3F^\circ$–^1G (40)	4026.1	19 100	1.56×10^{16}	2.15		−0.1		D	[1]
	$^1F^\circ$–^3G (58)	4552.5	19 100	1.56×10^{16}	0.75		−0.1		D	[1]
			19 600	3.3×10^{17}	1.3		0.15		D	[1]
			22 000	1.0×10^{17}	1.79		0.0*		C	[2]
			18 300	4.84×10^{17}	2.42				C	[4]
	$^1F^\circ$–^1G (59)	4530.4	19 100	1.56×10^{17}	2.5		−0.2		D	[1]
			22 000	1.0×10^{17}	2.20		−0.3		C	[2]
			22 800	1.0×10^{17}	2.2				C+	[3]

* Accuracy applies to width only.

N III

Ground State $1s^2 2s^2 2p\ ^2P^\circ_{1/2}$

Ionization Potential 47.448 eV 382704 cm^{-1}

The single experimental paper [1] reports measurements of Stark broadening parameters of four N III lines obtained in a low-pressure pulsed arc. However, there are no theoretical data available for comparison with the experiment.

Reference

[1] Popovic, M. Platisa, M. and Konjevic, N., Astron. Astrophys. **41**, 463 (1975).

Key data on experiments

Ref.	Plasma source	Method of measurement		Remarks
		Electron density	Temperature	
[1]	Low-pressure pulsed arc	Laser interferometry at 6328 Å	Boltzmann plot of relative N II line intensities.	

Numerical results for N III

Transition array	Multiplet (No.)	Wavelength Å	Temperature (K)	Electron density (cm^{-3})	w_m(Å)	w_m/w_{th}	d_m(Å)	d_m/d_{th}	Acc.	Ref.
1. $3s-(^1S)3p$	$^2S-^2P^\circ$ (1)	4097.3	24 300	5.5×10^{16}	0.096				C+	[1]
2. $3p-(^1S)3d$	$^2P^\circ-^2D$ (2)	4634.2	24 300	5.5×10^{16}	0.11				C+	[1]
		4640.6	24 300	5.5×10^{16}	0.12				C+	[1]
3. $2s2p3s-2s2p(^3P^\circ)3p$	$^4P^\circ-^4D$ (5)	3367.4	24 300	5.5×10^{16}	0.098				C+	[1]

6.13 Oxygen

O II

Ground State $1s^2 2s^2 2p^3\ ^4S^\circ_{3/2}$

Ionization Potential 35.116 eV = 283240 cm^{-1}

The data obtained by Platisa et al. [1] with a low-pressure pulsed arc are the only available source. The agreement with the semiclassical theory is very satisfactory, and data for different lines within multiplets are also very consistent.

Reference

[1] Platisa, M., Popovic, M., and Konjevic, N., to be published in Astron. Astrophys.

Key data on experiments

Ref.	Plasma source	Method of measurement		Remarks
		Electron density	Temperature	
[1]	Low pressure pulsed arc	Laser interferometry at 6328 Å	Boltzmann plot of O II line intensities.	

Numerical results for O II

Transition array	Multiplet (No.)	Wavelength Å	Temperature (K)	Electron density (cm^{-3})	w_m(Å)	w_m/w_{th}	d_m(Å)	d_m/d_{th}	Acc.	Ref.
1. $2p^2 3s-2p^2(^3P)3p$	$^4P-^4D^\circ$ (1)	4649.1	25 900	5.2×10^{16}	0.12	0.69			B	[1]
		4650.8	25 900	5.2×10^{16}	0.12	0.72			B	[1]
	$^4P-^4P^\circ$ (2)	4366.9	25 900	5.2×10^{16}	0.12	0.93			B	[1]
		4317.1	25 900	5.2×10^{16}	0.11	0.92			B	[1]
	$^4P-^4S^\circ$ (3)	3712.8	25 900	5.2×10^{16}	0.11	1.09			B	[1]
		3727.3	25 900	5.2×10^{16}	0.10	1.03			B	[1]
	$^2P-^2D^\circ$ (5)	4414.9	25 900	5.2×10^{16}	0.14	0.93			B	[1]

Numerical results for O II – Continued

Transition array	Multiplet (No.)	Wavelength Å	Temperature (K)	Electron density (cm^{-3})	w_m(Å)	w_m/w_{th}	d_m(Å)	d_m/d_{th}	Acc.	Ref.
	$^2P-^2P^\circ$ (6)	3973.3	25 900	5.2×10^{16}	0.12				B	[1]
2. $2p^23s'-2p^2(^1D)3p'$	$^2D-^2F^\circ$ (15)	4591.0	25 900	5.2×10^{16}	0.13				B	[1]
		4596.2	25 900	5.2×10^{16}	0.13				B	[1]
	$^2D-^2D^\circ$ (16)	4347.4	25 900	5.2×10^{16}	0.11				B	[1]
	$^2D-^2P^\circ$ (17)	3912.0	25 900	5.2×10^{16}	0.12				B	[1]
	$^2S^\circ-^2P$ (9)	3390.3	25 900	5.2×10^{16}	0.12				B	[1]
		3377.2	25 900	5.2×10^{16}	0.12				B	[1]
	$^4D^\circ-^4F$ (10)	4075.9	25 900	5.2×10^{16}	0.12	0.87			B	[1]
		4092.9	25 900	5.2×10^{16}	0.12	0.87			B	[1]
		4072.1	25 900	5.2×10^{16}	0.12	0.84			B	[1]
	$^4P^\circ-^4P$ (19)	4153.3	25 900	5.2×10^{16}	0.13	0.92			B	[1]
		4132.8	25 900	5.2×10^{16}	0.13	0.91			B	[1]
3. $2p^23p'-2p^2(^1D)3d'$	$^2F^\circ-^2G$ (36)	4185.5	25 900	5.2×10^{16}	0.10				B	[1]
4. $2p^23p-2p^2(^3P)4s$	$^4D^\circ-^4P$ (14)	3138.4	25 900	5.2×10^{16}	0.18	0.79			B	[1]

O III

Ground State $1s^22s^22p^2\ ^3P_0$

Ionization Potential 54.934 eV = 443086 cm^{-1}

The data obtained by Platisa et al. [1] with a low-pressure pulsed arc are the only source, and no semi-classical calculations exist for comparison.

Reference

[1] Platisa, M., Popovic, M., and Konjevic, N., to be published in Astron. Astrophys.

Key data on experiments

Ref.	Plasma source	Method of measurement		Remarks
		Electron density	Temperature	
[1]	Low-pressure pulsed arc	Laser interferometry at 6328 Å	Boltzmann plot of O III line intensities.	

Numerical results for O III

Transition array	Multiplet (No.)	Wavelength Å	Temperature (K)	Electron density (cm^{-3})	w_m(Å)	w_m/w_{th}	d_m(Å)	d_m/d_{th}	Acc.	Ref.
1. $2p3s-2p(^2P^\circ)3p$	$^3P^\circ-^3D$ (2)	3754.7	25 900	5.2×10^{16}	0.076				C+	[1]
		3759.9	25 900	5.2×10^{16}	0.072				C+	[1]
	$^3P^\circ-^3P$ (4)	3047.1	25 900	5.2×10^{16}	0.056				C+	[1]

Numerical results for O III – Continued

Transition array	Multiplet (No.)	Wavelength Å	Temperature (K)	Electron density (cm^{-3})	w_m(Å)	w_m/w_{th}	d_m(Å)	d_m/d_{th}	Acc.	Ref.
2. $2p3p-2p(^2P^\circ)3d$	$^3D-^3F^\circ$	3261.0	25 900	5.2×10^{16}	0.666				C+	[1]
	(8)	3265.5	25 900	5.2×10^{16}	0.063				C+	[1]
	$^3P-^3D^\circ$ (14)	3715.1	25 900	5.2×10^{16}	0.074				C+	[1]

6.14. Phosphorus

P II

Ground State $1s^22s^22p^63s^23p^2\ ^3P_0$

Ionization Potential 19.73 eV = 159100 cm^{-1}

Only one experimental paper deals with the Stark broadening of singly ionized phosphorus lines [1]. The results are reported normalized to the electron density 1.0×10^{17} cm^{-3}, although they were taken at densities between 3×10^{16} and 6×10^{16} cm^{-3}. It should be noted that in these measurements the instrumental profile (≈4 Å width) was several times wider than the Stark widths derived by Voigt analysis, which is the principal reason for the estimated low accuracy of these data.

References

[1] Miller, M. H., University of Maryland Technical Note BN-550 (1968).

Key data on experiments

Ref.	Plasma source	Method of measurement		Remarks
		Electron density	Temperature	
[1]	Gas driven shock tube	H_β Stark width	Absolute line intensity of Ne 5852 Å line H_β; line reversal technique applied to H_α	Photographic technique; low spectral resolution (≈4 Å).

Numerical results for P II

Transition array	Multiplet (No.)	Wavelength Å	Temperature (K)	Electron density (cm^{-3})	w_m(Å)	w_m/w_{th}	d_m(Å)	d_m/d_{th}	Acc.	Ref.
1. $3p4s-3p(^2P^\circ)4p$	$^3P^\circ-^3P$	5425.9	12 000	1.0×10^{17}	0.7	0.49			D	[1]
		5386.9	12 000	1.0×10^{17}	0.6	0.42			D	[1]
		5499.7	12 000	1.0×10^{17}	1.0	0.70			D+	[1]
		5409.7	12 000	1.0×10^{17}	0.7	0.49			D	[1]
		5316.1	12 000	1.0×10^{17}	0.9	0.63			D	[1]
	$^3P^\circ-^3S$	5191.4	12 000	1.0×10^{17}	1.9	1.57			C	[1]
	$^1P^\circ-^1D$	5253.5	12 000	1.0×10^{17}	0.8				D	[1]
2. $3p4p-3p(^4P^\circ)5s$	$^5D-^5P^\circ$	4943.5	12 000	1.0×10^{17}	1.9	1.16			C	[1]

6.15. Silicon

Si II

Ground State $1s^22s^22p^63s^23p\ ^2P^\circ_{1/2}$

Ionization Potential 16.345 eV = 131838.4 cm^{-1}

Three different spectroscopic sources and various plasma diagnostic techniques were applied to determine the Stark widths and shifts of some prominent Si II lines [1–5].

It is interesting to note that according to the comparisons of compiled data, good mutual agreement of

experimental results is obtained for the Si II multiplets 1 and 2, but unusually large discrepancies exist with the theory.

References

[1] Miller, M. H., University of Maryland Technical Note BN-550 (1968).
[2] Konjevic, N., Puric, J., Cirkovic, Lj., and Labat, J., J. Phys. **B3**, 999 (1970).
[3] Chapelle, J., and Czernichowski, A., Acta Phys. Pol. **41**, 753 (1972).
[4] Puric, J., Djenize, S., Labat, J., and Cirkovic, Lj., Phys. Lett. **45A**, 97 (1973).
[5] Puric, J., Djenize, S., Labat, J., and Cirkovic, Lj., Z. Phys. **267**, 71 (1974).

Key data on experiments

Ref.	Plasma source	Method of measurement		Remarks
		Electron density	Temperature	
[1]	Gas driven shock tube	H_β Stark width	Absolute intensities of the Ne 5852 Å line and H_β; line reversal technique applied to H_α	Photographic technique; low spectral resolution (4 Å).
[2]	T-tube	Laser interferometry at 6328 Å and 1.15 μm	Boltzmann plot of Ar II line intensities	
[3]	Plasma jet	H_α Stark width	Plasma composition data	
[4–5]	T-tube	Laser interferometry at 6328 Å	Boltzmann plot of Ar II line intensities	

Numerical results for Si II

Transition array	Multiplet (No.)	Wavelength Å	Temperature (K)	Electron density (cm^{-3})	w_m(Å)	w_m/w_{th}	d_m(Å)	d_m/d_{th}	Acc.	Ref.
1. $3s3p^2-3s^2(^1S)4p$	$^2D-^2P^\circ$ (1)	3856.0	8500–9700	$(1.82–2.40)\times10^{17}$	0.73–0.91	0.33–0.33			C+	[2]
			8700–16 400	1.0×10^{17}	0.52–0.60	0.43–0.54	0.03–0.06	(*)	C+	[4], [5]
		3862.6	8500–9700	$(1.82–2.40)\times10^{17}$	0.76–1.01	0.35–0.36			C+	[2]
			8700–16 400	1.0×10^{17}	0.44–0.48	0.37–0.51	0.03–0.06	(*)	C+	[4], [5]
2. $3s^24s-3s^2(^1S)4p$	$^2S-^2P^\circ$ (2)	6347.1	8500–10 000	1.82×10^{17}	2.44	0.55			C+	[2]
				1.0×10^{17}	1.1	0.47			B	[3]
		6371.4	8500–10 000	1.82×10^{17}	2.34	0.53			C+	[2]
				1.0×10^{17}	1.15	0.49			B	[3]
			8700–16 400	1.0×10^{17}	1.00–0.82	0.41–0.40	(−0.12)–(−0.16)	0.11–0.19	C+	[4], [5]
3. $3s^24p-3s^2(^1S)4d$	$^2P^\circ-^2D$ (5)	5041.0	10 000	1.0×10^{17}	3.0	1.03			C	[1]
4. $3s^24p-3s^2(^1S)5s$	$^2P^\circ-^2S$ (4)	5979.0	10 000	1.0×10^{17}	2.4	0.93			C	[1]
5. $3s3p4s-3s3p(^3P^\circ)4p$	$^4P^\circ-^4P$ (8)	5868.4	8500	1.82×10^{17}	2.18				C+	[2]

(*) Theory predicts opposite sign.

Si III

Ground State $1s^22s^22p^63s^2\,{}^1S_0$

Ionization Potential 33.492 eV = 270139.3 cm^{-1}

The T-tube measurements by Puric et al. [1], which are the only available source, have been compared with the semiempirical Gaunt-factor approximation [2]. The experimental Stark widths are smaller by about 30 percent. No semiclassical calculations are available.

References

[1] Puric, J., Djenize, S., Labat, J., and Cirkovic, Lj., Z. Phys. **267**, 71 (1974).
[2] Griem, H. R., Phys. Rev. **165**, 258 (1968).

Key data on experiments

Ref.	Plasma source	Method of measurement		Remarks
		Electron density	Temperature	
[1]	T-tube	Laser interferometry at 6328 Å	Boltzmann plot of Ar II line intensities	No corrections for Doppler and instrumental broadening reported.

Numerical results for Si III

Transition array	Multiplet (No.)	Wavelength Å	Temperature (K)	Electron density (cm^{-3})	w_m(Å)	w_m/w_{th}	d_m(Å)	d_m/d_{th}	Acc.	Ref.
1. $3s4s-3s(^2S)4p$	$^3S-^3P^o$ (2)	4552.6	8700–16 400	1.0×10^{17}	0.48–0.38		0.05–0.05		C	[1]
		4567.8	8700	1.0×10^{17}	0.56		0.04		C	[1]
			10 600–16 400	1.0×10^{17}			0.04–0.07		C	[1]
2. $3s4d-3s(^2S)5f$	$^3D-^3F^o$ (8.06)	3486.9	8700–16 400	1.0×10^{17}			0.04–0.06		C	[1]

6.16. Strontium

Sr II

Ground State $1s^22s^22p^63s^23p^63d^{10}4s^24p^65s\ ^2S_{1/2}$

Ionization Potential 11.030 eV = 88964.0 cm^{-1}

Only three experimental papers are available on the Stark broadening of Sr II lines [1–3]. One of those papers [3] was excluded from further consideration since the work was repeated and corrected by some of these authors [2]. The large discrepancy between the two sets of results [2] and [3] is most probably due to incorrect treatment of the optical depths in ref. [3].

However, the line shift data from the T-tube experiment [1, 3] agree well with those obtained from the pulsed arc [2], since the shift measurements are essentially not affected by self-absorption problems.

References

[1] Puric, J., and Konjevic, N., Z. Phys. **249**, 440 (1972).
[2] Hadziomerspahic, D., Platisa, M., Konjevic, N., and Popovic, M., Z. Phys. **262**, 169 (1973).
[3] Puric, J., Platisa, M., and Konjevic, N., Z. Phys. **247**, 216 (1971)

Key data on experiments

Ref.	Plasma source	Method of measurement		Remarks
		Electron density	Temperature	
[1]	T-tube	Laser interferometry at 6328 Å	Boltzmann plot of Ar II line intensities	
[2]	Z-pinch	Laser interferometry at at 6328 Å	Boltzmann plot of Ar II line intensities	(Shift measurements only)

Numerical results for Sr II

Transition array	Multiplet (No.)	Wavelength Å	Temperature (K)	Electron density (cm^{-3})	w_m(Å)	w_m/w_{th}	d_m(Å)	d_m/d_{th}	Acc.	Ref.
1. $4p^65s-4p^6(^1S)5p$	$^2S-^2P^o$ (1)	4077.7	14 200	1.0×10^{17}			−0.09		C	[1]
			31 700	1.0×10^{17}	0.22				B	[2]
		4215.5	14 200	1.0×10^{17}			−0.09		C	[1]
			31 700	1.0×10^{17}	0.24				B	[2]

Numerical results for Sr II – Continued

Transition array	Multiplet (No.)	Wavelength Å	Temperature (K)	Electron density (cm^{-3})	w_m(Å)	w_m/w_{th}	d_m(Å)	d_m/d_{th}	Acc.	Ref.
2. $4p^65p$–$4p^6(^1S)5d$	$^2P°$–^2D (2)	3380.7	14 200	1.0×10^{17}			0.24		C+	[1]
			31 700	1.0×10^{17}			0.27		C+	[2]
		3464.5	14 200	1.0×10^{17}			0.29		C+	[1]
			31 700	1.0×10^{17}			0.27		C+	[2]
3. $4p^65p$–$4p^6(^1S)6s$	$^1P°$–^1S (3)	4161.8	14 200	1.0×10^{17}			0.19		C+	[1]
			31 700	1.0×10^{17}			0.18		C+	[2]
		4305.5	14 200	1.0×10^{17}			0.19		C+	[1]

6.17. Sulphur

S II

Ground State $1s^22s^22p^63s^23p^3\ {}^4S°_{3/2}$

Ionization Potential 23.33 eV = 188200 cm^{-1}

While two different plasma sources were used for investigations of S II line widths, both experiments were performed at the same temperature and similar electron densities [1, 2]. The agreement between these two sets of experimental data is well within the limits of experimental error. The only exception is the measured width for the 4815.5 Å S II line from ref. [2]. This line is much wider than one would expect on the basis of comparisons with other, similar type transitions. However, the author of ref. [2] noticed an interference with the 4817.3 Å line of C I; therefore, the estimated accuracy for this line has been lowered to the range of D.

References

[1] Bridges, J. M., and Wiese, W. L., Phys. Rev. **159**, 31 (1967).
[2] Miller, M. H., University of Maryland Technical Note BN-550 (1968).

Key data on experiments

Ref.	Plasma source	Method of measurement		Remarks
		Electron density	Temperature	
[1]	Wall-stabilized arc	H_β Stark width	Absolute intensities of O I lines and plasma composition data	
[2]	Gas driven shock tube	H_β Stark width	Absolute intensity of Ne I 5852 Å line and H_β: line reversal technique applied to H_α	Photographic technique; low spectral resolution (1 Å).

Numerical results for S II

Transition array	Multiplet (No.)	Wavelength Å	Temperature (K)	Electron density (cm^{-3})	w_m(Å)	w_m/w_{th}	d_m(Å)	d_m/d_{th}	Acc.	Ref.
1. $3s3p^4$–$3s^23p^24p$	^2P–$^2S°$ (1)	5027.2	11 100	7.0×10^{16}	0.39	0.91			B	[1]
			11 000	1.0×10^{17}	0.51	0.83			C	[2]
2. $3p^23d$–$3p^2(^3P)4p$	^4F–$^4D°$ (11)	5606.1	11 100	7.0×10^{16}	0.37				B	[1]
			11 000	1.0×10^{17}	0.55				C	[2]
		5660.0	11 000	1.0×10^{17}	0.67				C	[2]

Numerical results for S II – Continued

Transition array	Multiplet (No.)	Wavelength Å	Temperature (K)	Electron density (cm^{-3})	w_m(Å)	w_m/w_{th}	d_m(Å)	d_m/d_{th}	Acc.	Ref.
3. $3p^24s$–$3p^2(^3P)4p$	^4P–$^4D^\circ$ (6)	5453.8	11 100	7.0×10^{16}	0.39	0.91			B	[1]
			11 000	1.0×10^{17}	0.47	0.77			C	[2]
		5432.8	11 100	7.0×10^{16}	0.42	0.98			B	[1]
			11 000	1.0×10^{17}	0.55	0.90			C	[2]
		5428.6	11 100	7.0×10^{16}	0.39	0.91			B	[1]
			11 000	1.0×10^{17}	0.45	0.74			C	[2]
		5509.7	11 100	7.0×10^{16}	0.42	0.98			B	[1]
			11 000	1.0×10^{17}	0.49	0.80			C	[2]
		5473.6	11 100	7.0×10^{16}	0.45	1.05			B	[1]
			11 000	1.0×10^{17}	0.55	0.90			C	[2]
		5564.9	11 000	1.0×10^{17}	0.60	0.98			C	[2]
	^4P–$^4P^\circ$ (7)	5103.3	11 000	1.0×10^{17}	0.75	1.56			C+	[2]
		5009.5	11 000	1.0×10^{17}	0.60	1.25			C	[2]
		5032.4	11 100	7.0×10^{16}	0.53	1.58			B	[1]
			11 000	1.0×10^{17}	0.68	1.42			C+	[2]
	^4P–$^4S^\circ$ (9)	4815.5	11 100	7.0×10^{16}	0.7				C+	[1]
			11 000	1.0×10^{17}	1.44				D	[2]
		4716.2	11 100	7.0×10^{16}	0.7				C+	[1]
	^2P–$^2P^\circ$ (15)	5014.0	11 000	1.0×10^{17}	0.80				C+	[2]
4. $3p^24s'$–$3p^2(^3P)4d$	^2D–$^2F^\circ$ (38)	5320.7	11 100	7.0×10^{16}	0.53				B	[1]
		5345.7	11 100	7.0×10^{16}	0.46				B	[1]
			11 000	1.0×10^{17}	0.62				C+	[2]
	^2D–$^2D^\circ$ (39)	5212.6	11 000	1.0×10^{17}	0.62				C+	[2]

6.18. Zinc

Zn II

Ground State $1s^22s^22p^63s^23p^63d^{10}4s\ ^2S_{1/2}$

Ionization Potential 17.964 eV = 144892.6 cm^{-1}

For the experimental data obtained with a pulsed discharge [1] no theoretical comparison values are available. Considering the high density conditions and rather large dimension of this discharge, self-absorption could be significant, but no check of it is reported.

References

[1] Kusch, H. J., and Oberschelp, E., Z. Astrophys. **67**, 77 (1967)

Key data on experiments

Ref.	Plasma source	Method of measurement		Remarks
		Electron density	Temperature	
[1]	Pulsed discharge	H_β Stark width	Plasma composition data	No self-absorption check reported; photographic technique.

Numerical results for Zn II

Transition array	Multiplet (No.)	Wavelength Å	Temperature (K)	Electron density (cm^{-3})	w_m(Å)	w_m/w_{th}	d_m(Å)	d_m/d_{th}	Acc.	Ref.
1. $4s4p$–$4s(^2S)5s$	$^2P^o$–^2S	2558.0	11 000	1.0×10^{17}	0.88				D	[1]
	(3 UV)	2502.0	11 000	1.0×10^{17}	0.64				D	[1]
2. $4s4d$–$4s(^2S)4f$	^2D–$^2F^o$	4924.0	11 000	1.0×10^{17}	2.55				D	[1]
	(3)	4911.7	11 000	1.0×10^{17}	2.45				D	[1]